CHAPTER IV

RESULTS AND DISCUSSION

4.1 Characterization of Benzoxazine Monomers

Structural characterization of 3,4-dihydro-3,6,8-trimethyl-2H-1,3-benzoxazine **1**, and 3,4-dihydro-3,6-dimethyl-2H-1,3-benzoxazine **2** were previously reported by Pongtamrug *et al.*

The prepared monomers **3-15** were characterized as follows. Each spectrum is shown in Figures 4.1-4.26.

3,4-dihydro-6-ethyl-3-methyl-2H-1,3-benzoxazine **3**

FTIR (KBr, cm^{-1}) : 1499 (vs, oxazine), 1229 (vs, C-O-C stretching), 1200 (s, C-N-C stretching), 1144 (s, C-H in-plane bending), 937 (s, C-H out of plane), 822 (s, C-H out of plane), 742 (m, C-C-C bending).

^{1}H-NMR (in $CDCl_3$) : δ 1.20 (3H, t, Ar-CH_2-**CH_3**), 2.50 (2H, q, Ar-**CH_2**-CH_3), 2.70 (3H, s, N-**CH_3**), 3.90 (2H, s, Ar-**CH_2**-N), 4.75 (2H, s, O-**CH_2**-N), 6.75 (1H, d, Ar-**H**), 6.85 (1H, s, Ar-**H**), 6.95 (1H, d, Ar-**H**)

% Yield = 65

TLC (R_f) = 0.45 (CH_3OH : $CHCl_3$; 1: 19).

3,4-dihydro-6-t-butyl-3-methyl-2H-1,3-benzoxazine **4**

FTIR (KBr, cm^{-1}) : 1502 (vs, oxazine), 1234 (vs, C-O-C stretching), 1143 (s, C-H in-plane bending), 938 (vs, C-H out of plane), 821 (s, C-H out of plane), 755 (m, C-C-C bending).

H-NMR (in $CDCl_3$) : δ 1.30 (9H, s, Ar-C(**CH_3**)$_3$), 3.93 (2H, s, Ar-**CH_2**-N), 4.75 (2H, s, O-**CH_2**-N), 6.72 (1H, d, Ar-**H**), 6.94 (1H, s, Ar-**H**), 7.15 (1H, d, Ar-**H**).

% Yield = 70

TLC (R_f) = 0.74 (CH_3OH : $CHCl_3$; 1: 19).

3,4-dihydro-3-methyl-2H-1,3-benzoxazine **5**

FTIR (KBr, cm^{-1}) : 1489 (vs, oxazine), 1231 (vs, C-O-C stretching), 1217 (s, C-N-C stretching), 1144 (s, C-H in-plane bending), 928 (vs, C-H out of plane), 862 (s, C-H out of plane), 755 (m, C-C-C bending).

^{1}H-NMR (in $CDCl_3$) : δ 2.60 (3H, s, N-**CH_3**), 3.95 (2H, s, Ar-**CH_2**-N), 4.78 (2H, s, O-**CH_2**-N), 6.77-6.94 (5H, m, Ar-**H**)

% Yield = 55

TLC (R_f) = 0.33 (CH_3OH : $CHCl_3$; 1: 19).

3,4-dihydro-6,8-dimethyl-3-propyl-2H-1,3-benzoxazine **6**

FTIR (KBr, cm^{-1}) : 1486 (vs oxazine), 1220 (vs, C-O-C stretching), 1201 (s, C-N-C stretching), 1144 (s, C-H in-plane bending), 928 (vs, C-H out of plane), 862 (s, C-H out of plane), 755 (vs, C-C-C bending).

^{1}H-NMR (in $CDCl_3$) : δ 0.91 (3H, t, N-CH_2-CH_2-**CH_3**), 1.57 (2H, m, N-CH_2-**CH_2**-CH_3), 2.13 (3H, s, Ar-**CH_3**), 2.20 (3H, s, Ar- **CH_3**), 2.68 (3H, t, N-**CH_2**-CH_2-CH_3), 3.92 (2H, s, Ar-**CH_2**-N), 4.84 (2H, s, O-**CH_2**-N), 6.59 (1H, s, Ar-**H**), 6.79 (1H, s, Ar-**H**).

% Yield = 90

TLC (R_f) = 0.50 (CH_3OH : $CHCl_3$; 1: 19).

3,4-dihydro-6-methyl-3-propyl-2H-1,3-benzoxazine **7**

FTIR (KBr, cm^{-1}) : 1502 (vs, oxazine), 1223 (vs, C-O-C stretching), 1143 (s, C-H in-plane bending), 940 (s, C-H out of plane), 815 (s, C-H out of plane).

^{1}H-NMR (in $CDCl_3$) : δ 1.23 (3H, t, N-CH_2-CH_2-**CH_3**), 1.63 (2H, m, N-CH_2-**CH_2**-CH_3), 2.23 (3H, s, Ar-**CH_3**), 2.69 (2H, t, N-**CH_2**-CH_2-CH_3), 4.04 (2H, s, Ar-**CH_2**-N), 4.94 (2H, s, O-**CH_2**-N), 6.64 (1H, d, Ar-**H**), 6.75 (1H, s, Ar-**H**), 6.87 (1H, d, Ar-**H**).

% Yield = 85

TLC (R_f) = 0.40 (CH_3OH : $CHCl_3$; 1: 19).

3,4-dihydro-6-ethyl-3-propyl-2H-1,3-benzoxazine **8**

FTIR (KBr, cm^{-1}) : 1500 (vs, oxazine), 1223 (vs, C-O-C stretching), 1143 (s, C-H in-plane bending), 938 (s, C-H out of plane), 821 (m, C-H out of plane).

^{1}H-NMR (in $CDCl_3$) : δ 1.19 (3H, t, N-CH_2-CH_2-**CH_3**), 1.26 (3H, t, Ar-CH_2-**CH_3**), 1.64 (2H, m, N-CH_2-**CH_2**-CH_3), 2.56 (2H, q, Ar-**CH_2**-CH_3), 2.64 (2H, t, N-**CH_2**-CH_2-CH_3), 4.00 (2H, s, Ar-**CH_2**-N), 4.88 (2H, s, O-**CH_2**-N), 6.64 (1H, d, Ar-**H**), 6.75 (1H, s, Ar-**H**), 6.87 (1H, d, Ar-**H**).

% Yield : 90

TLC (R_f) = 0.46 (CH_3OH : $CHCl_3$; 1: 19).

3,4-dihydro-6-t-butyl-3-propyl-2H-1,3-benzoxazine **9**

FTIR (KBr, cm^{-1}) : 1503 (vs, oxazine), 1231 (vs, C-O-C stretching), 1203 (m, C-N-C stretching), 1142 (s, C-H in-plane bending), 937 (s, C-H out of plane), 822 (s, C-H out of plane), 750 (m, C-C-C bending).

^{1}H-NMR (in $CDCl_3$) : δ : 0.97 (3H, t, N-CH_2-CH_2-**CH_3**), 1.28 (9H, s, Ar-C(**CH_3**)$_3$), 1.52 (2H, m, N-CH_2-**CH_2**-CH_3), 2.65 (2H, t, N-**CH_2**-CH_2-CH_3), 3.98 (2H, s, Ar-**CH_2**-N), 4.83 (2H, s, O-**CH_2**-N), 6.77-7.15 (4H, m, Ar-**H**)

% Yield = 60

TLC (R_f) = 0.76 (CH_3OH : $CHCl_3$; 1: 19).

3,4-dihydro-3-propyl-2H-1,3-benzoxazine **10**

FTIR (KBr, cm^{-1}) : 1489 (vs, oxazine), 1224 (vs, C-O-C stretching), 1141 (s, C-H in-plane bending), 937 (vs, C-H out of plane), 754 (vs, C-C-C bending).

^{1}H-NMR (in $CDCl_3$) : δ 0.93 (3H, t, N-CH_2-CH_2-**CH_3**), 1.60 (2H, m, N-CH_2-**CH_2**-CH_3), 2.71 (2H, t, N-**CH_2**-CH_2-CH_3), 3.99 (2H, s, Ar-**CH_2**-N), 4.87 (2H, s, O-**CH_2**-N), 6.75-7.11 (5H, m, Ar-**H**).

% Yield = 65

TLC (R_f) = 0.35 (CH_3OH : $CHCl_3$; 1: 19).

3,4-dihydro-6,8-dimethyl-3-cyclohexyl-2H-1,3-benzoxazine **11**

FTIR (KBr, cm^{-1}) : 1486 (vs, oxazine), 1222 (vs, C-O-C stretching), 1197 (m, C-N-C stretching), 1149 (s, C-H in-plane bending), 923 (s, C-H out of plane), 851 (m, C-H out of plane).

^{1}H-NMR (in $CDCl_3$) : δ 1.23 (2H, m, **CH_2** of cyclohexyl group), 1.72 (4H, m, **CH_2** of cyclohexyl group), 1.94 (4H, dt, **CH_2** of cyclohexyl group), 2.11 (3H, s, Ar-**CH_3**), 2.20 (3H, s, Ar- **CH_3**), 2.85 (1H, t, **CH** of cyclohexyl group), 4.01 (2H, s, Ar-**CH_2**-N), 4.95 (2H, s, O-**CH_2**-N), 6.59 (1H, s, Ar-**H**), 6.76 (1H, s, Ar-**H**).

% Yield = 90

TLC (R_f) = 0.54 (CH_3OH : $CHCl_3$; 1: 19).

3,4-dihydro-6-methyl-3-cyclohexyl-2H-1,3-benzoxazine **12**

FTIR (KBr, cm^{-1}) : 1502 (vs, oxazine), 1226 (vs, C-O-C stretching), 1149 (s, C-H in-plane bending), 935 (s, C-H out of plane), 814 (s, C-H out of plane).

^{1}H-NMR (in $CDCl_3$) : δ 1.15 (2H, m, **CH_2** of cyclohexyl group), 1.23 (4H, m, **CH_2** of cyclohexyl group), 1.75 (4H, dt, **CH** of cyclohexyl group), 4.05 (2H, s, Ar-**CH_2**-N), 4.95 (2H, s, O-**CH_2**-N), 6.65 (1H, d, Ar-**H**), 6.75 (1H, s, Ar-**H**), 6.85 (1H, d, Ar-**H**).

% Yield = 85

TLC (R_f) = 0.44 (CH_3OH : $CHCl_3$; 1: 19).

3,4-dihydro-6-ethyl-3-cyclohexyl-2H-1,3-benzoxazine **13**

FTIR (KBr, cm^{-1}) : 1500 (vs, oxazine), 1227 (vs, C-O-C stretching), 1149 (s, C-H in-plane bending), 935 (s, C-H out of plane), 814 (s, C-H out of plane).

^{1}H-NMR (in $CDCl_3$) : δ 1.13 (3H, t, Ar-CH_2-**CH_3**), 1.18 (2H, m, **CH_2** of cyclohexyl group), 1.24 (4H, m, **CH_2** of cyclohexyl group), 1.73 (4H, dt, **CH_2** of cyclohexyl group), 2.69 (1H, t, **CH** of cyclohexyl group), 4.05 (2H, s, Ar-**CH_2**-N), 4.94 (2H, s, O-**CH_2**-N), 6.65 (1H, d, Ar-**H**), 6.78 (1H, s, Ar-**H**), 6.89 (1H, d, Ar-**H**).

% Yield = 90

TLC (R_f) = 0.48 (CH_3OH : $CHCl_3$; 1: 19).

3,4-dihydro-6-t-butyl-3-cyclohexyl-2H-1,3-benzoxazine **14**

FTIR (KBr, cm^{-1}) : 1501 (vs, oxazine), 1230 (vs, C-O-C stretching), 1203 (m, C-N-C stretching), 1131 (s, C-H in-plane bending), 923 (vs, C-H out of plane), 822 (vs, C-H out of plane), 745 (m, C-C-C bending).

^{1}H-NMR (in $CDCl_3$) : δ 1.15-1.23 (6H, m, **CH_2** of cyclohexyl group), 1.30 (9H, s, Ar-**$C(CH_3)_3$**), 1.75 (4H, dt, **CH** of cyclohexyl group), 2.70 (1H, t, **CH** of cyclohexyl group), 4.09 (2H, s, Ar-**CH_2**-N), 4.95 (2H, s, O-**CH_2**-N), 6.65 (1H, d, Ar-**H**), 6.95 (1H, s, Ar-**H**), 7.10 (1H, d, Ar-**H**).

% Yield = 75

TLC (R_f) = 0.78 (CH_3OH : $CHCl_3$; 1: 19).

3,4-dihydro-3-cyclohexyl-2H-1,3-benzoxazine **15**

FTIR (KBr, cm^{-1}) : 1489 (vs, oxazine), 1226 (vs, C-O-C stretching), 1188 (vs, C-N-C stretching), 1149 (vs, C-H in-plane bending), 921 (vs, C-H out of plane), 843 (s, C-H out of plane), 753 (vs, C-C-C bending).

^{1}H-NMR (in $CDCl_3$) : δ 1.18 (2H, m, **CH_2** of cyclohexyl group), 1.49 (4H, m, **CH_2** of cyclohexyl group), 1.75 (4H, dt, **CH_2** of cyclohexyl group), 2.68 (1H, t, **CH** of cyclohexyl group), 4.07 (2H, s, Ar-**CH_2**-N), 4.97 (2H, s, O-**CH_2**-N), 6.71-7.13 (5H, m, Ar-**H**).

% Yield = 80

TLC (R_f) = 0.39 (CH_3OH : $CHCl_3$; 1: 19).

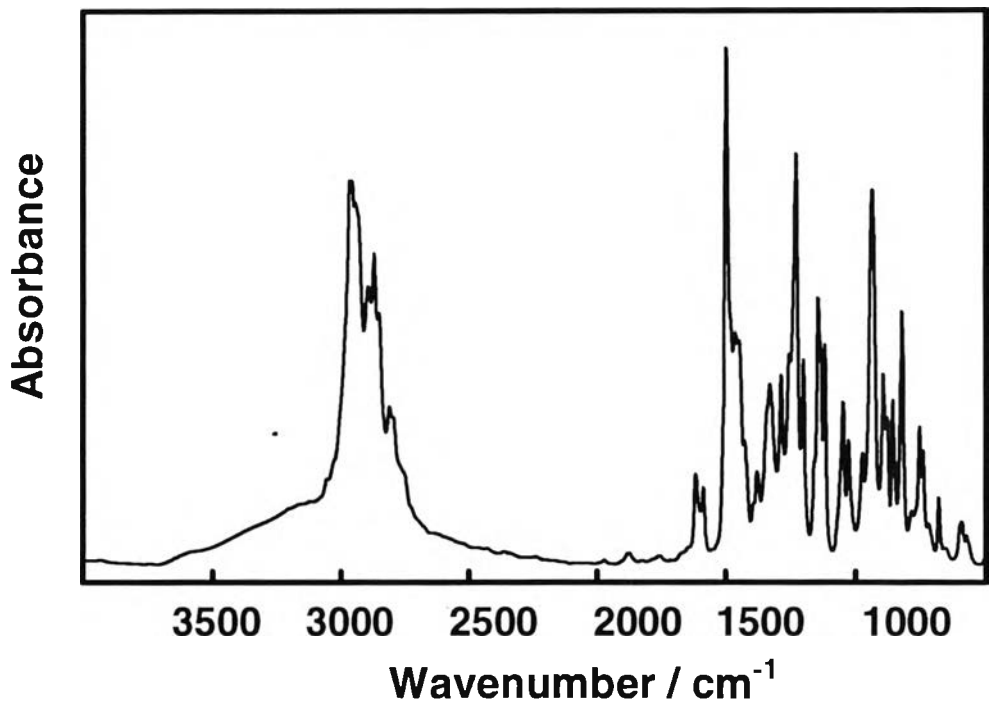

Figure 4.1 FTIR spectrum of **3**.

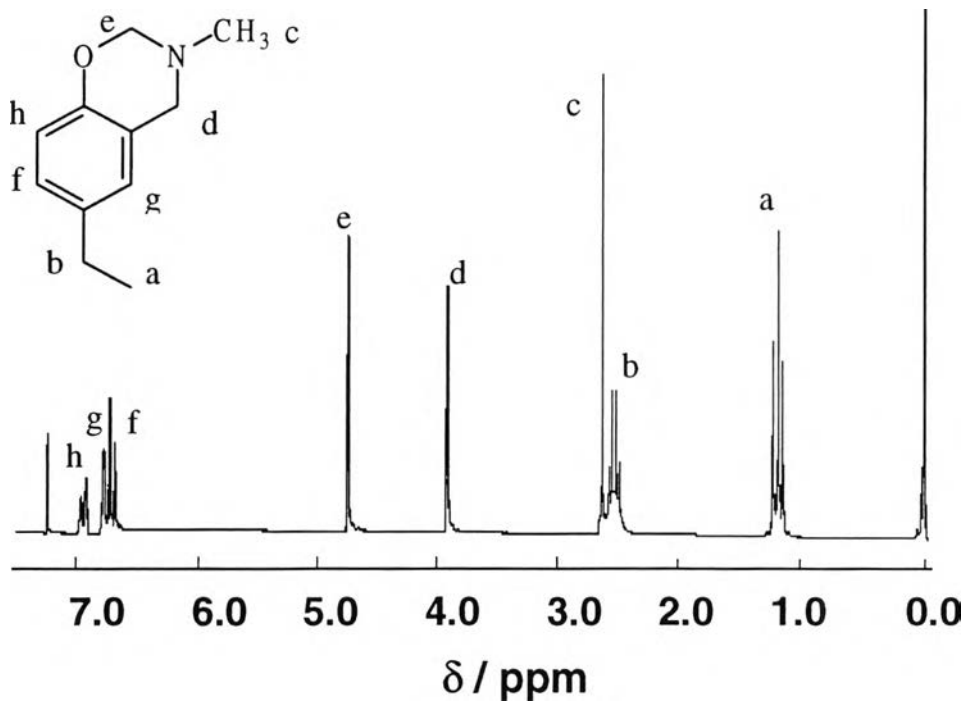

Figure 4.2 ^{1}H-NMR spectrum of **3**.

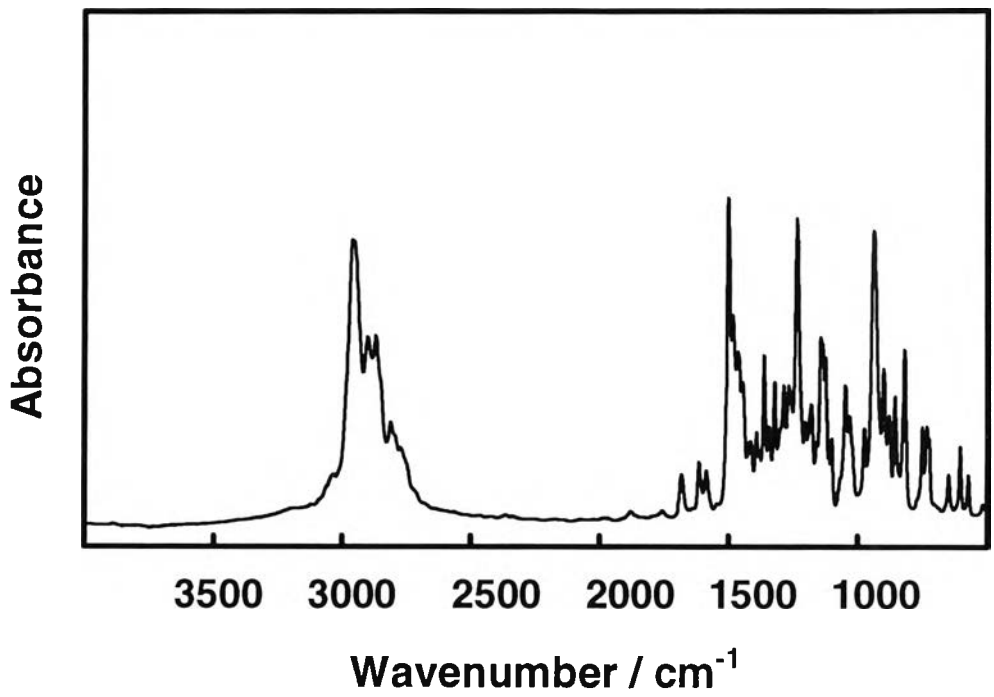

Figure 4.3 FTIR spectrum of **4**.

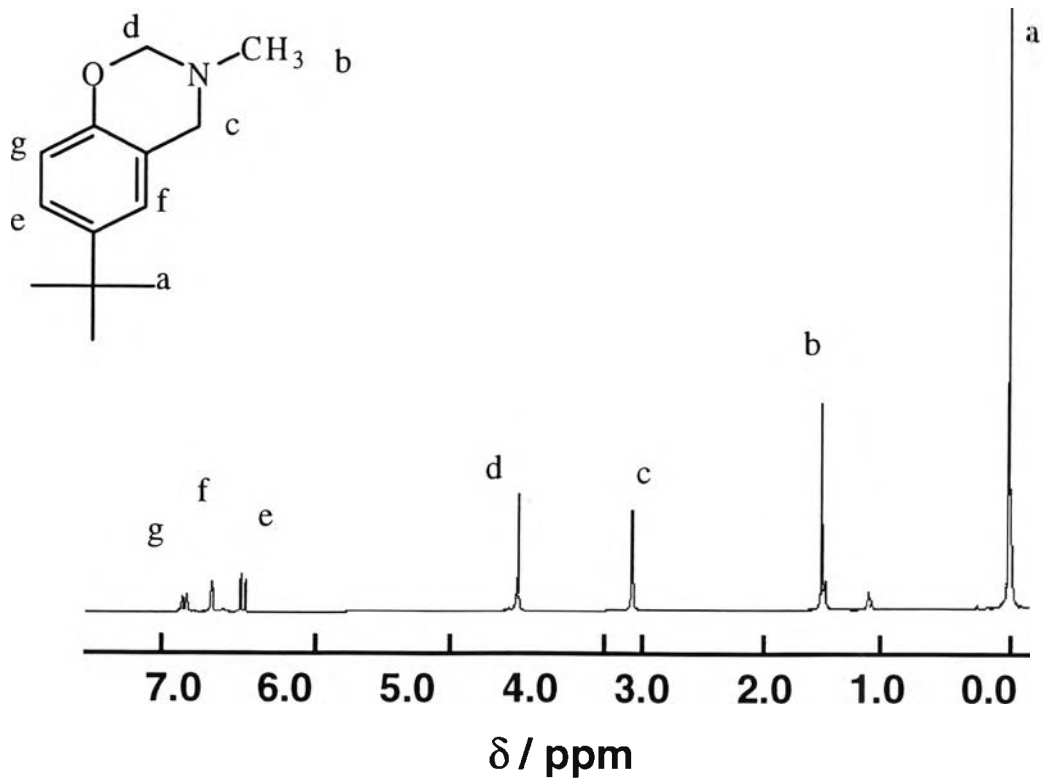

Figure 4.4 ^{1}H-NMR spectrum of **4**.

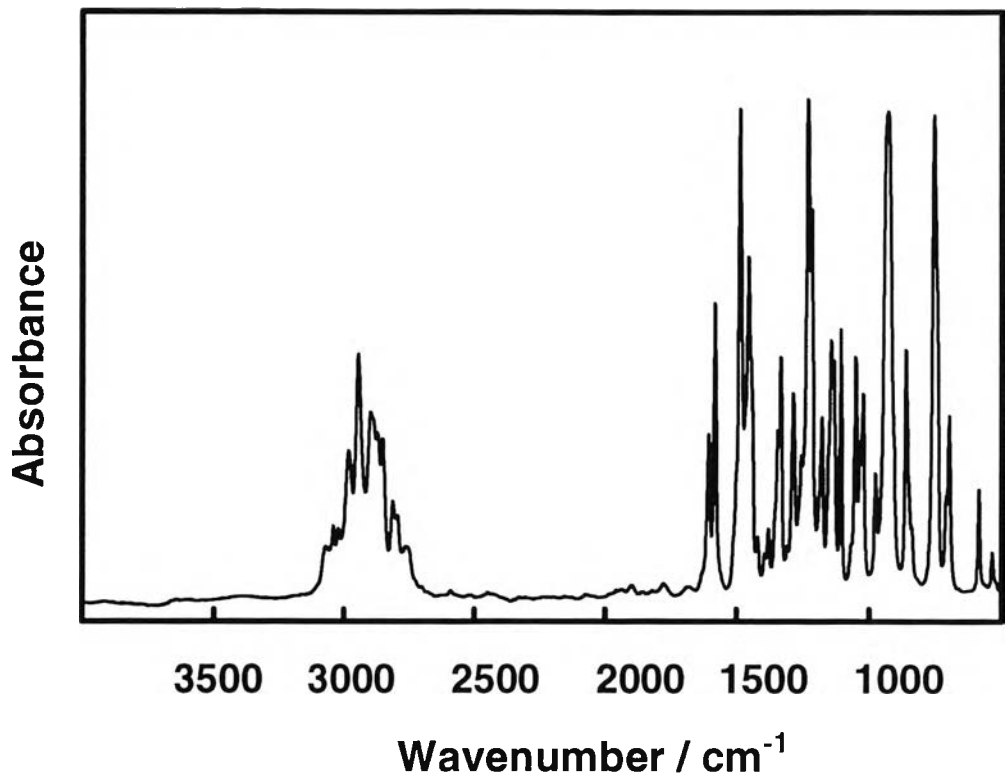

Figure 4.5 FTIR spectrum of **5**.

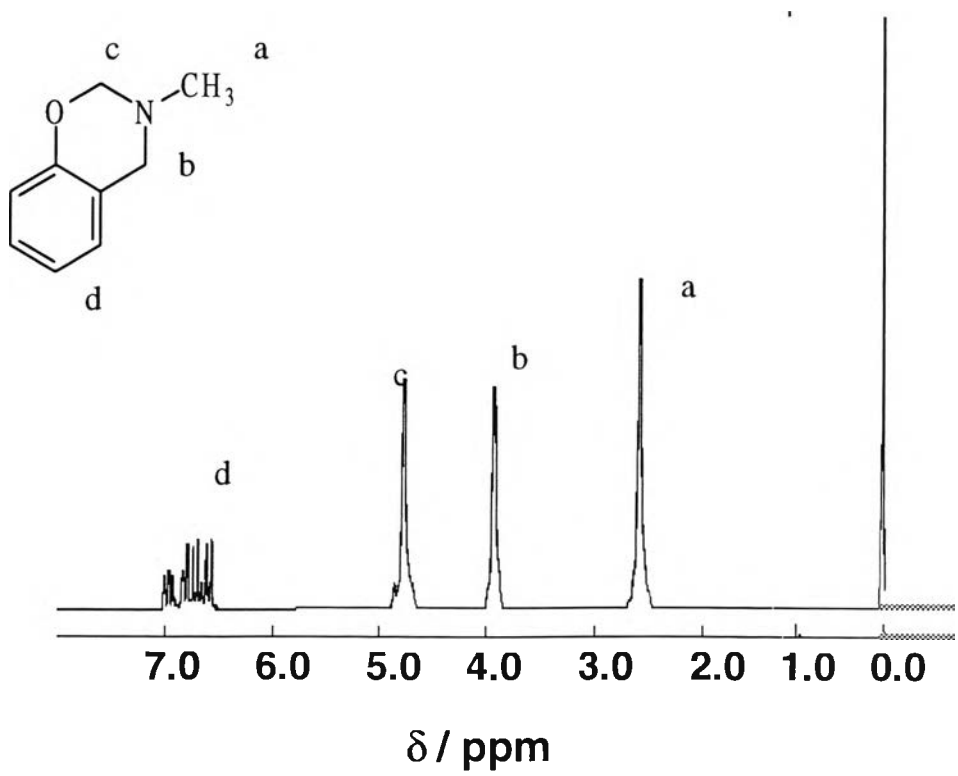

Figure 4.6 ^{1}H-NMR spectrum of **5**.

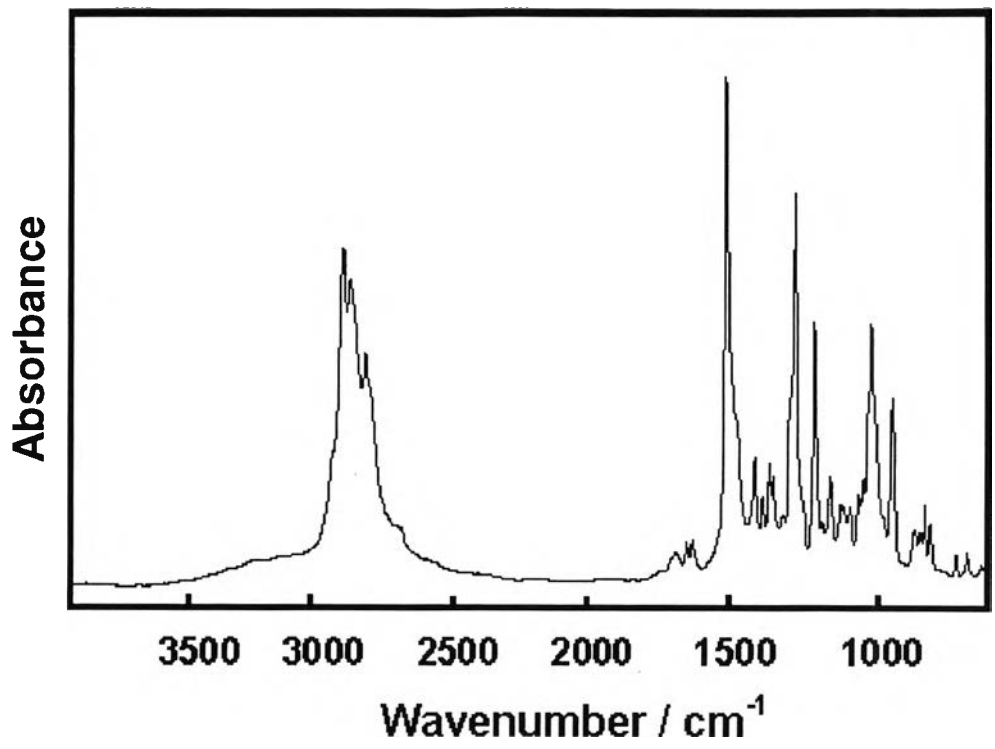

Figure 4.7 FTIR spectrum of **6**.

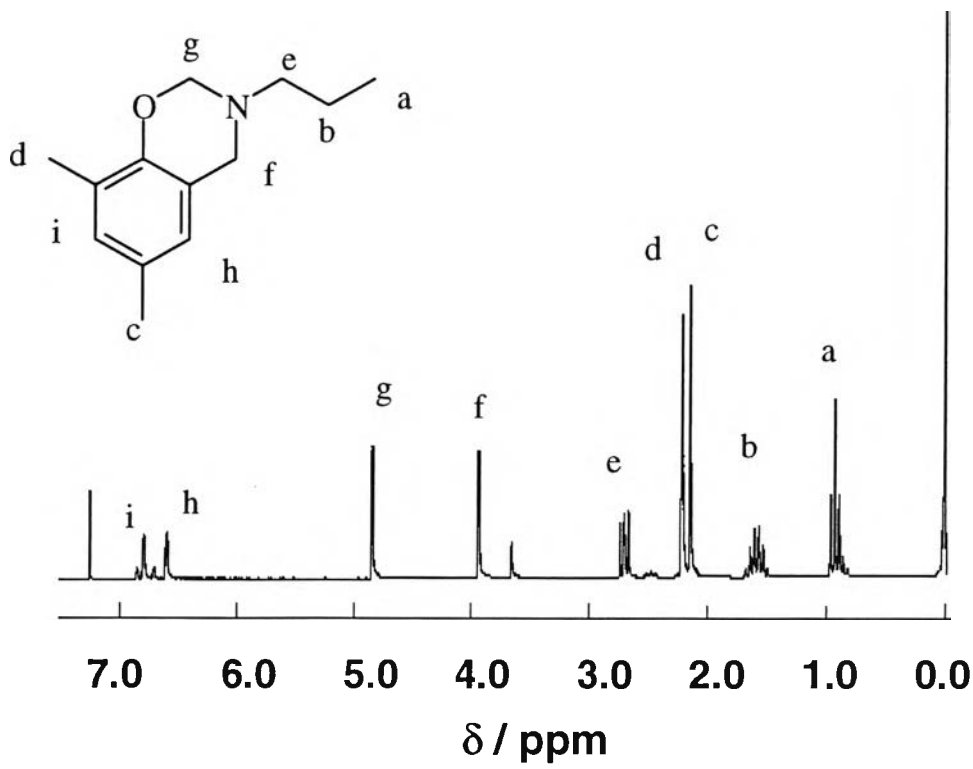

Figure 4.8 ^{1}H-NMR spectrum of **6**.

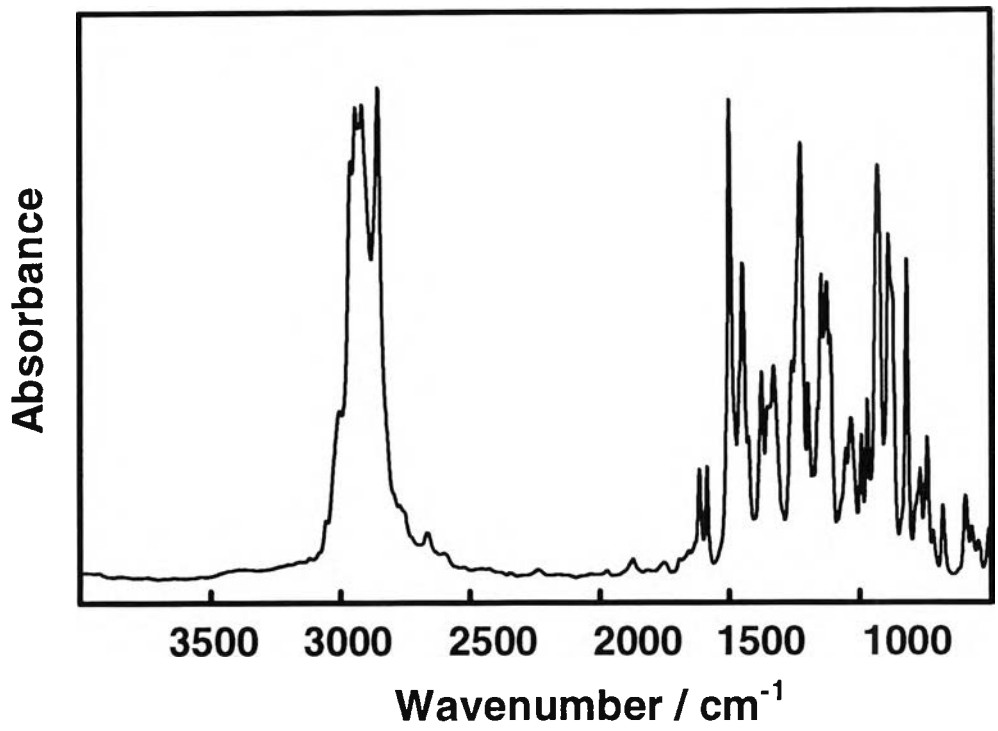

Figure 4.9 FTIR spectrum of **7**.

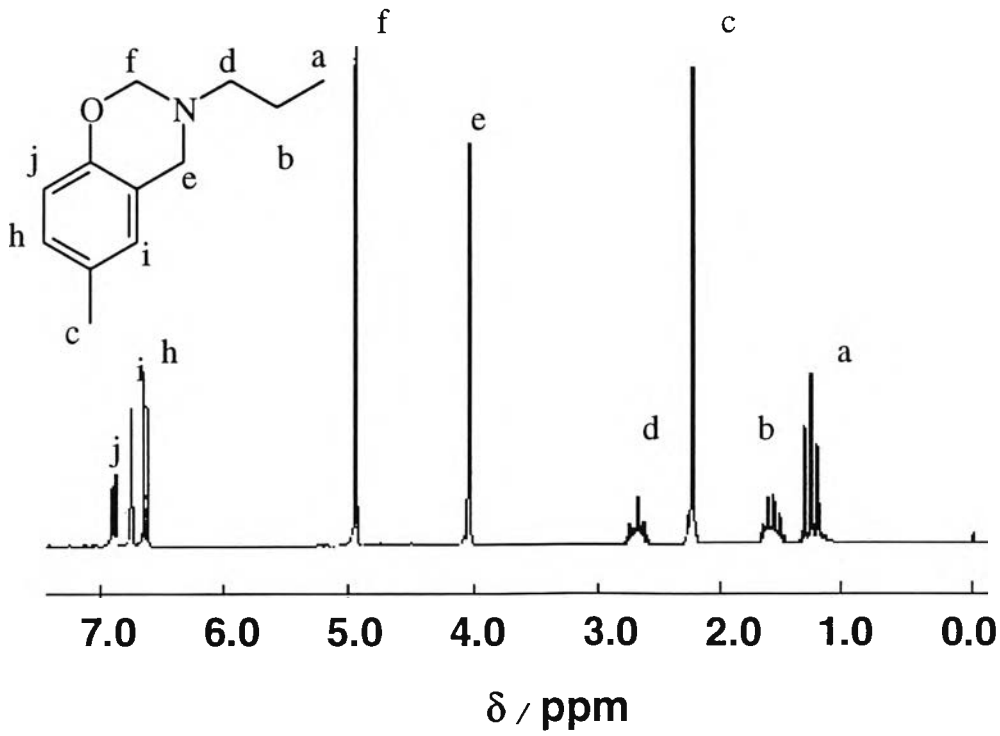

Figure 4.10 ^{1}H-NMR spectrum of **7**.

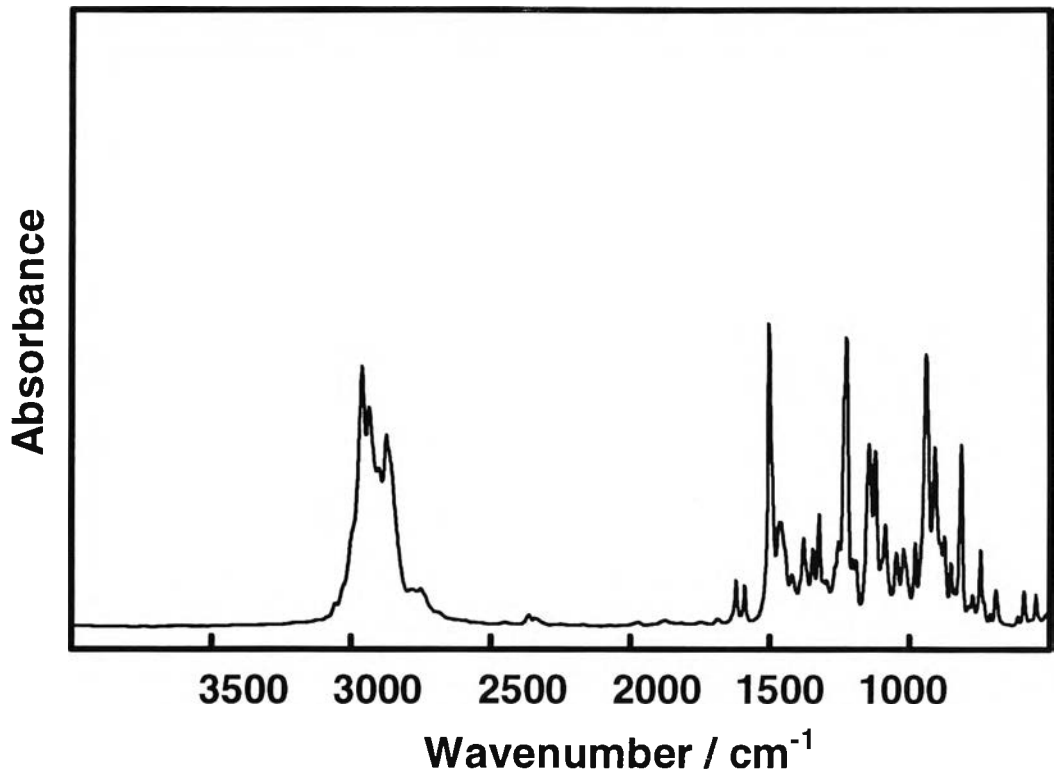

Figure 4.11 FTIR spectrum of **8**.

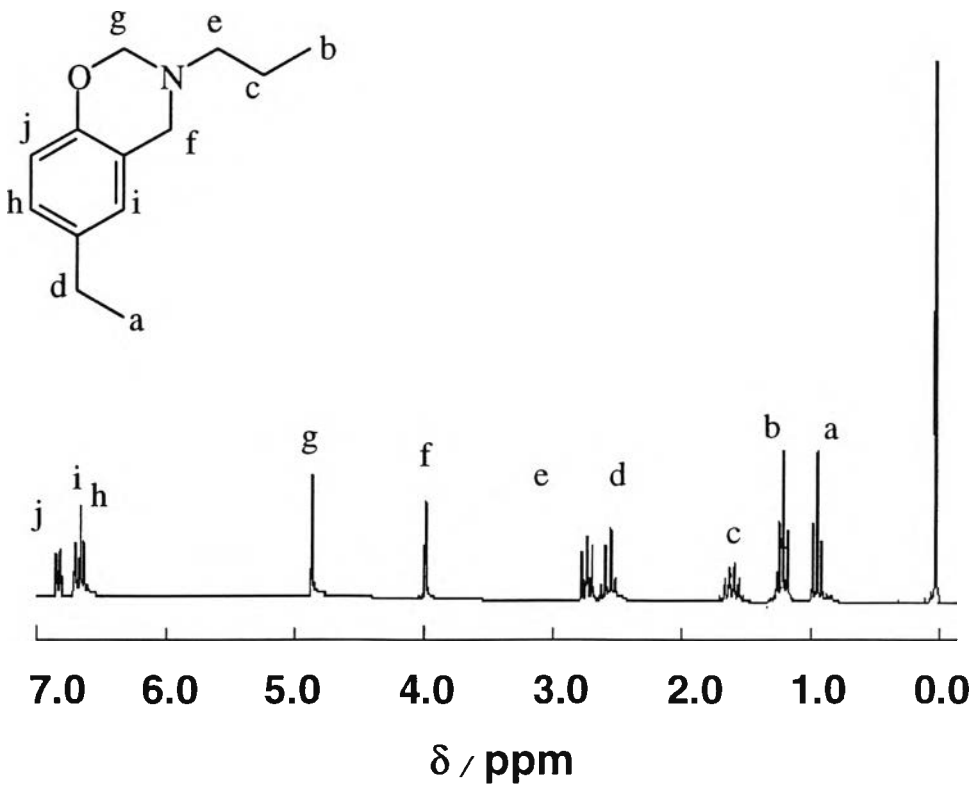

Figure 4.12 ^{1}H-NMR spectrum of **8**.

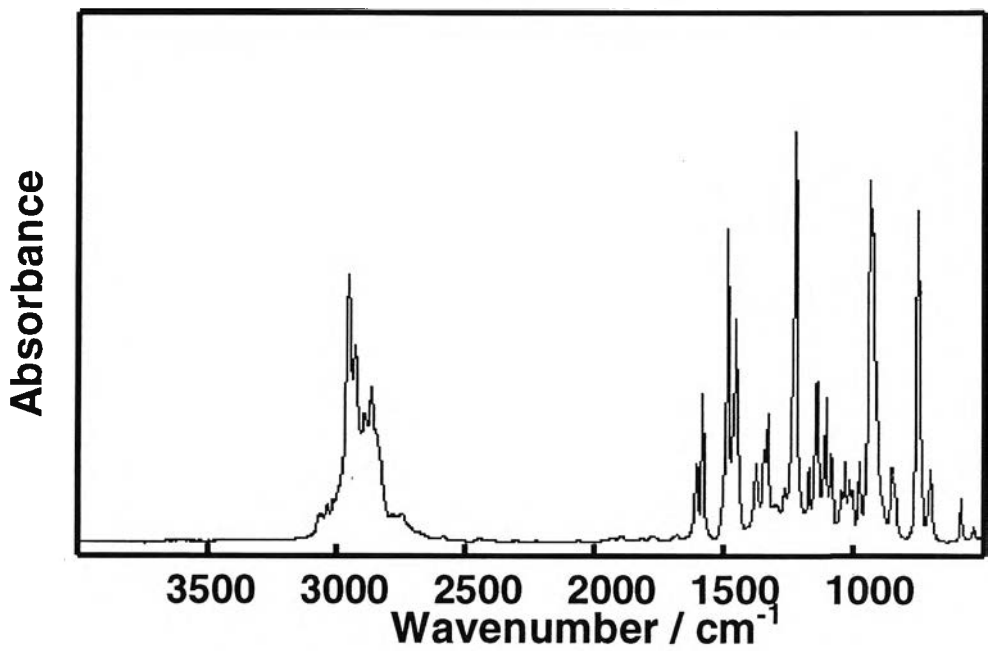

Figure 4.13 FTIR spectrum of **9**.

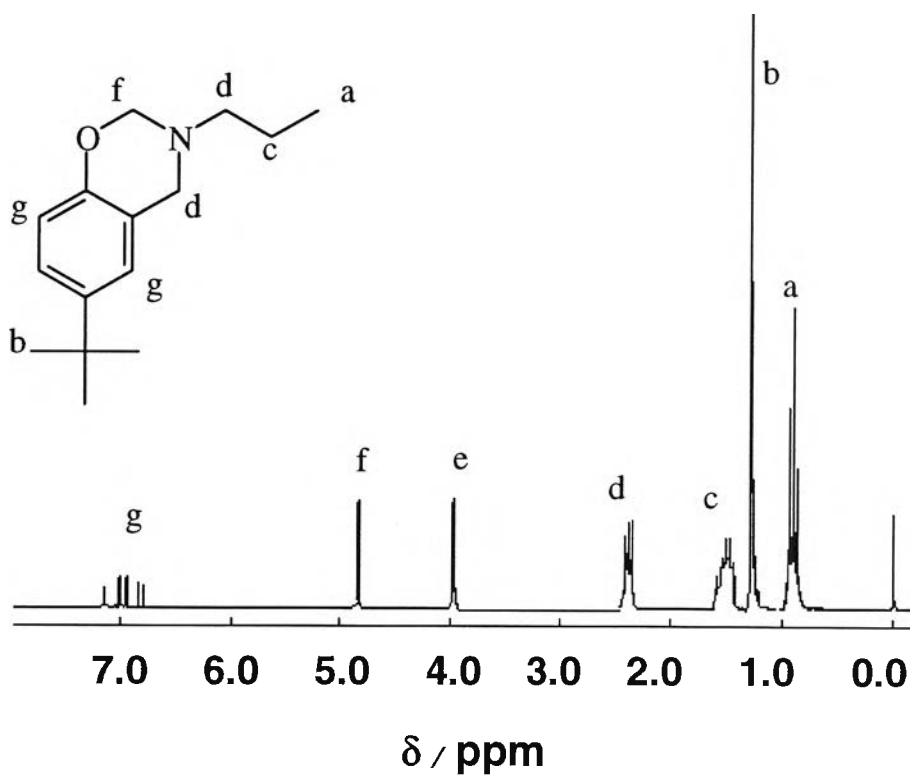

Figure 4.14 FTIR spectrum of **9**.

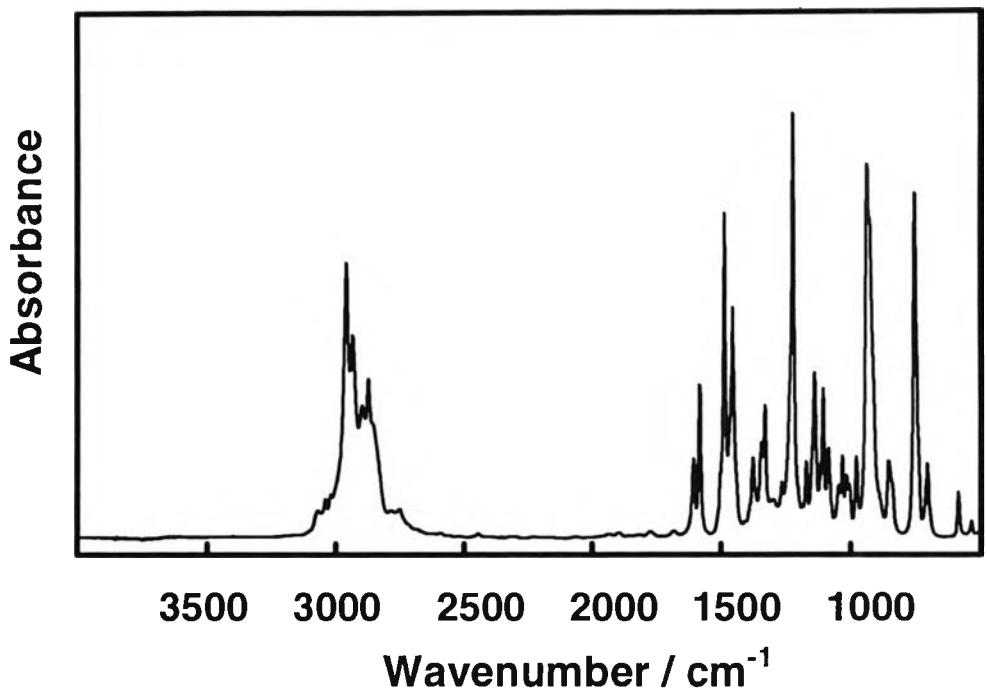

Figure 4.15 FTIR spectrum of **10**.

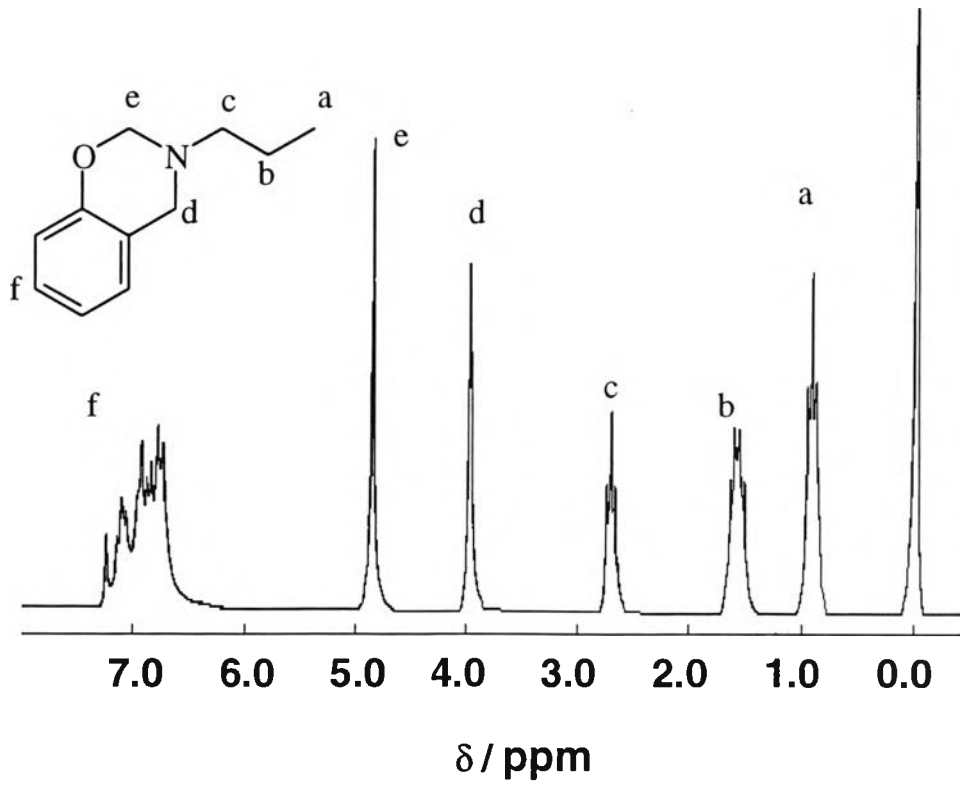

Figure 4.16 ^{1}H-NMR spectrum of **10**.

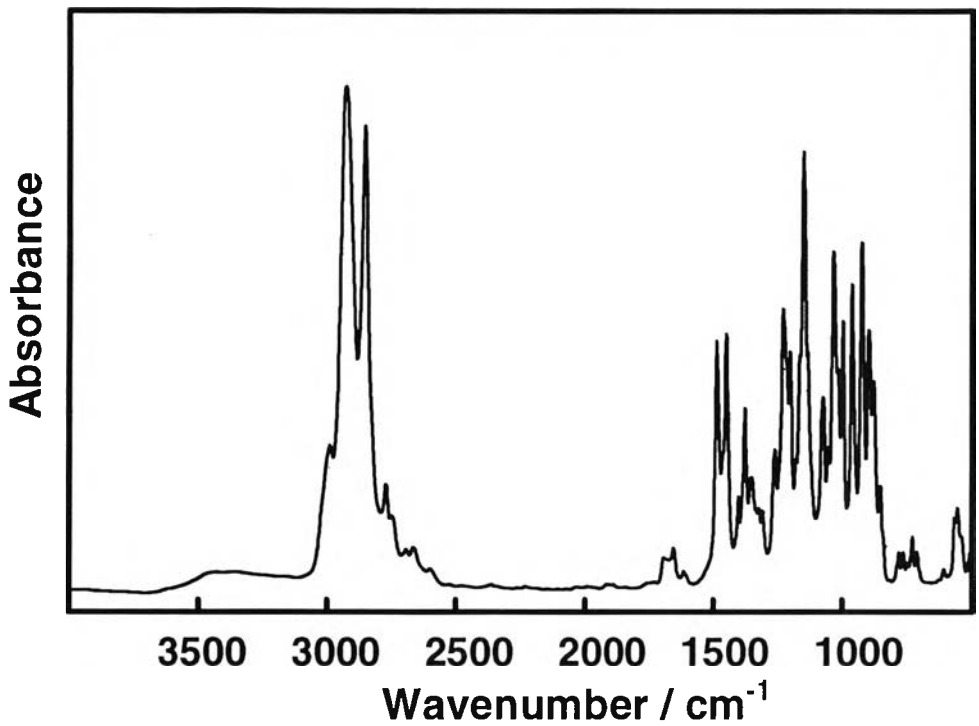

Figure 4.17 FTIR spectrum of **11**.

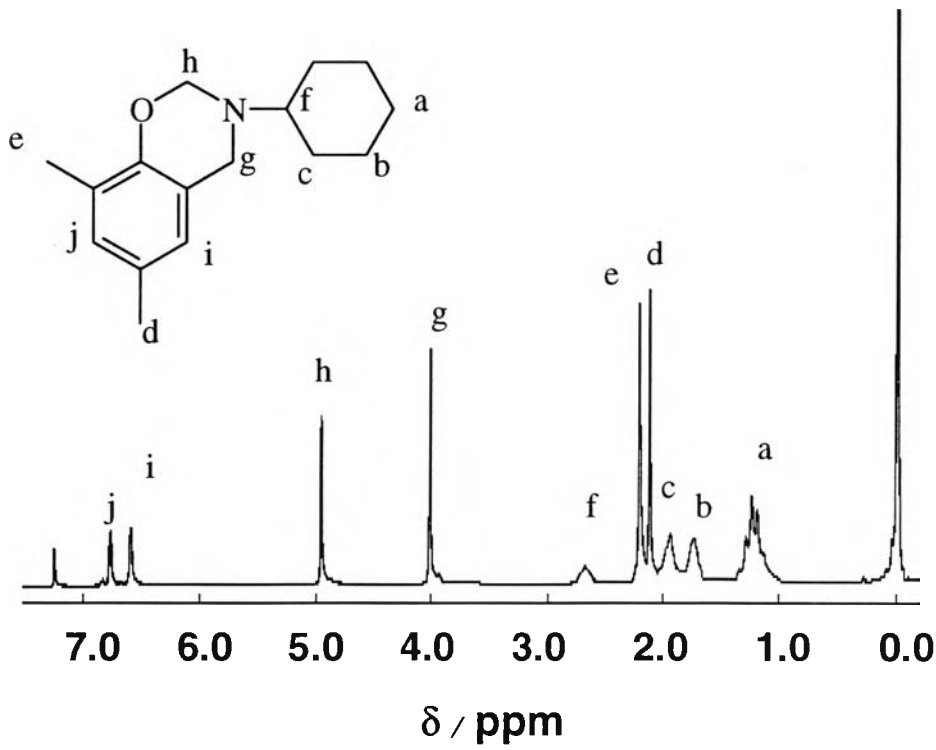

Figure 4.18 ^{1}H-NMR spectrum of **11**.

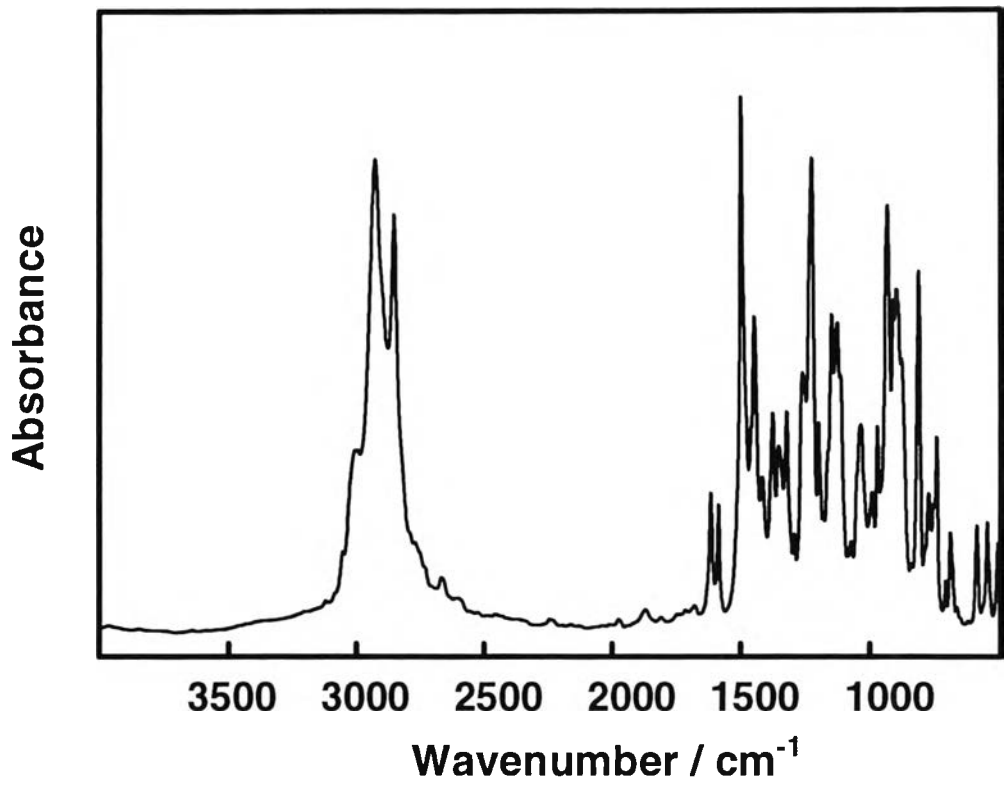

Figure 4.19 FTIR spectrum of **12**.

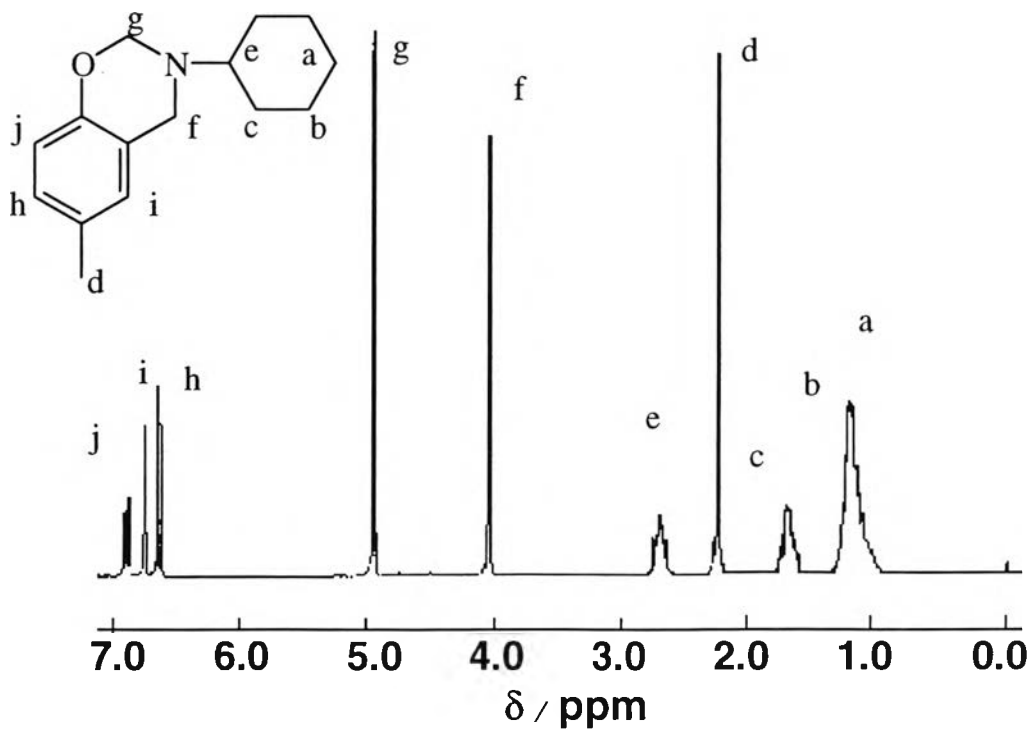

Figure 4.20 ^{1}H-NMR spectrum of **12**.

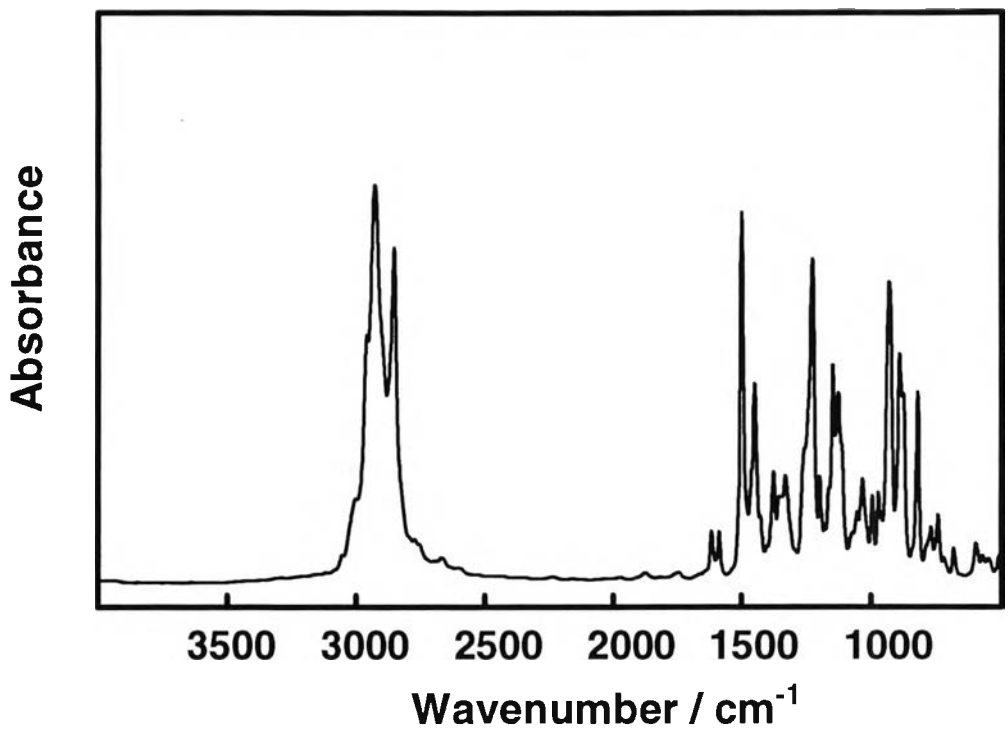

Figure 4.21 FTIR spectrum of **13**.

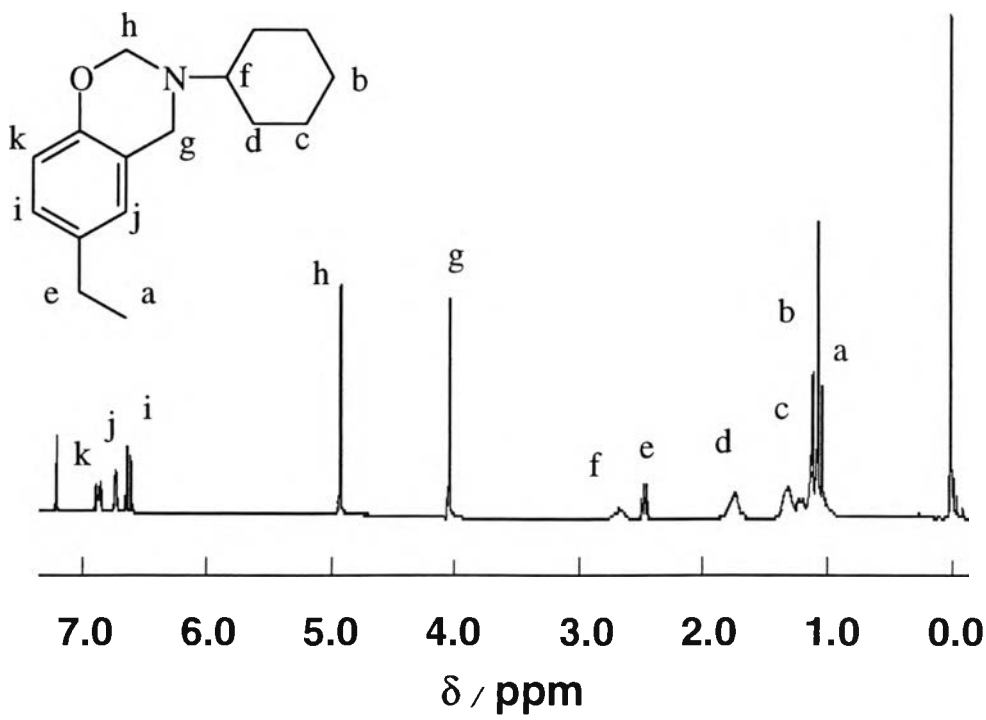

Figure 4.22 ^{1}H-NMR spectrum of **13**.

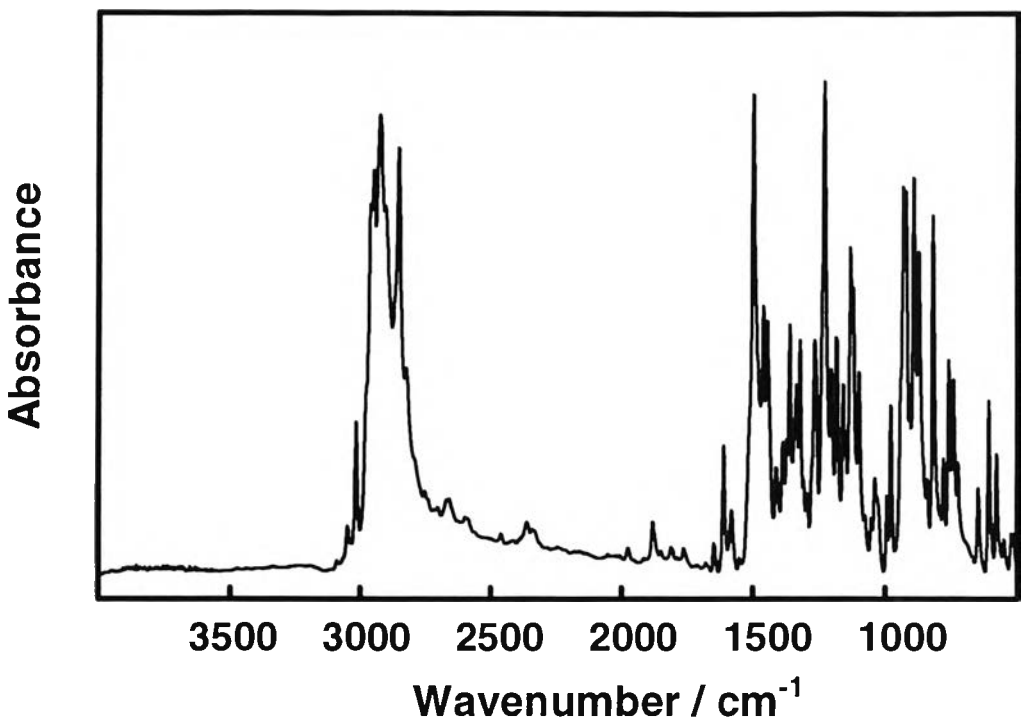

Figure 4.23 FTIR spectrum of **14**.

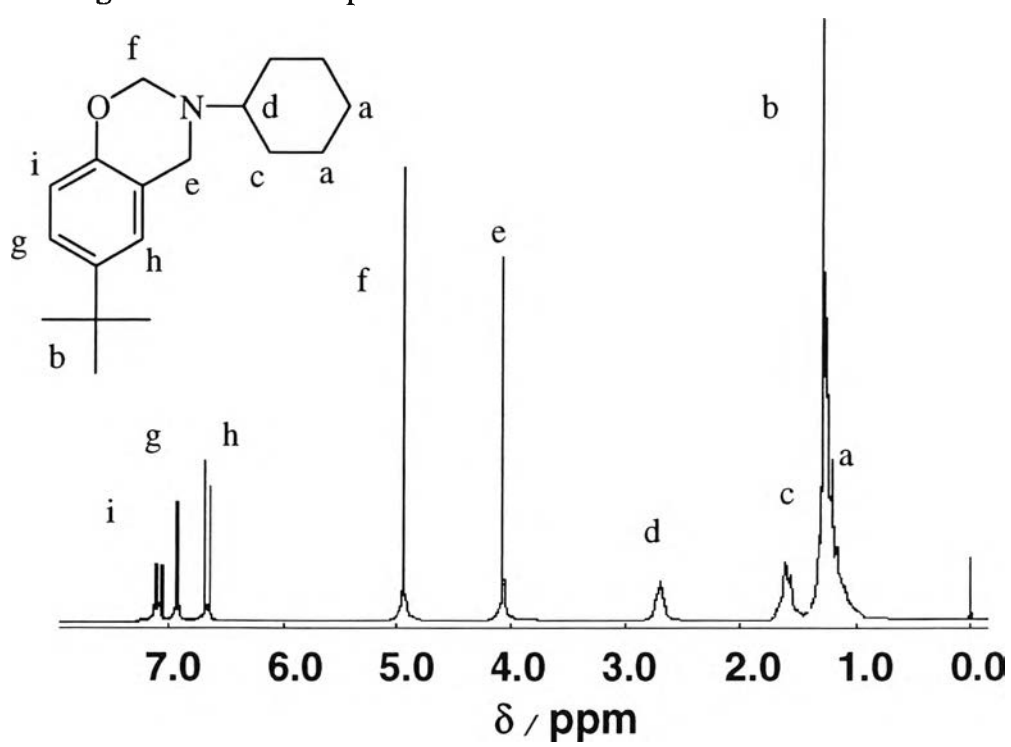

Figure 4.24 ^{1}H-NMR spectrum of **14**.

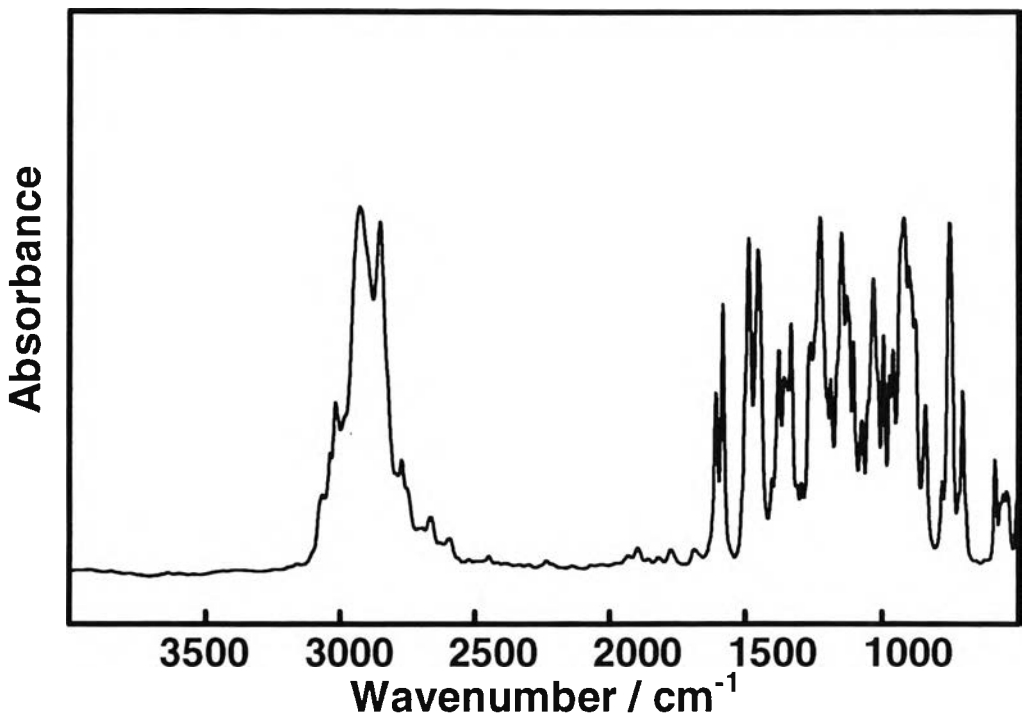

Figure 4.25 FTIR spectrum of **15**.

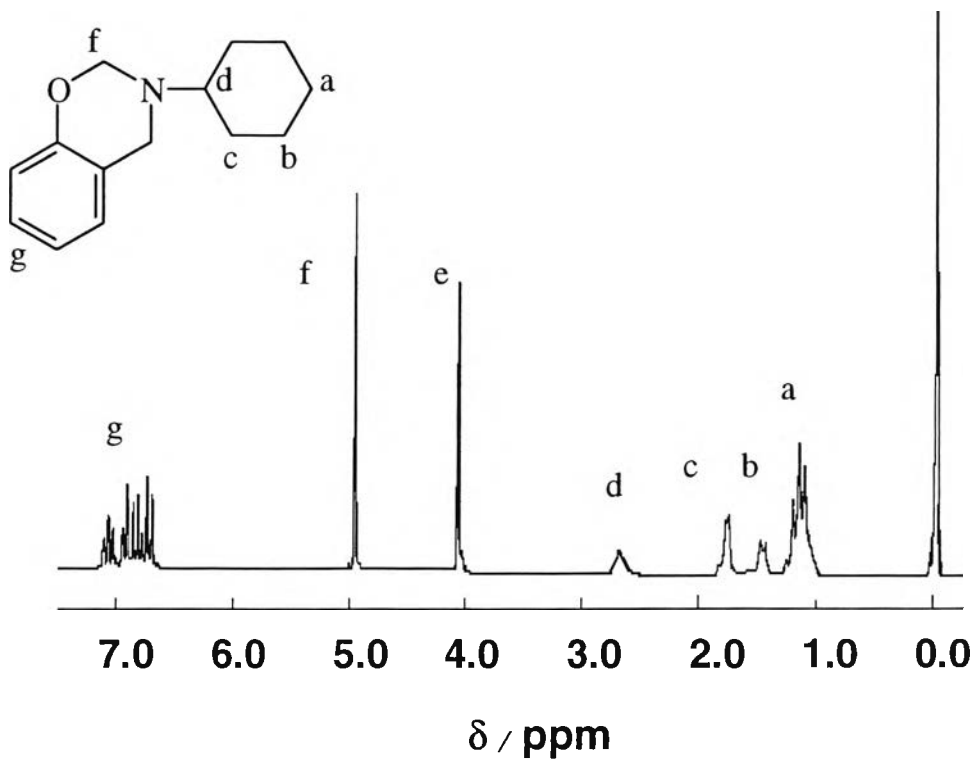

Figure 4.26 ^{1}H-NMR spectrum of **15**.

4.2 Ion Interaction of Benzoxazine Monomer Derivatives

Benzoxazine monomers are expected to give a specific conformation as a host compound to form complexes with guest molecules, especially, ion guests. The ion extraction percentage was studied by variation of concentrations, and the structures.

4.2.1 Effect of Benzoxazine Monomer Concentration

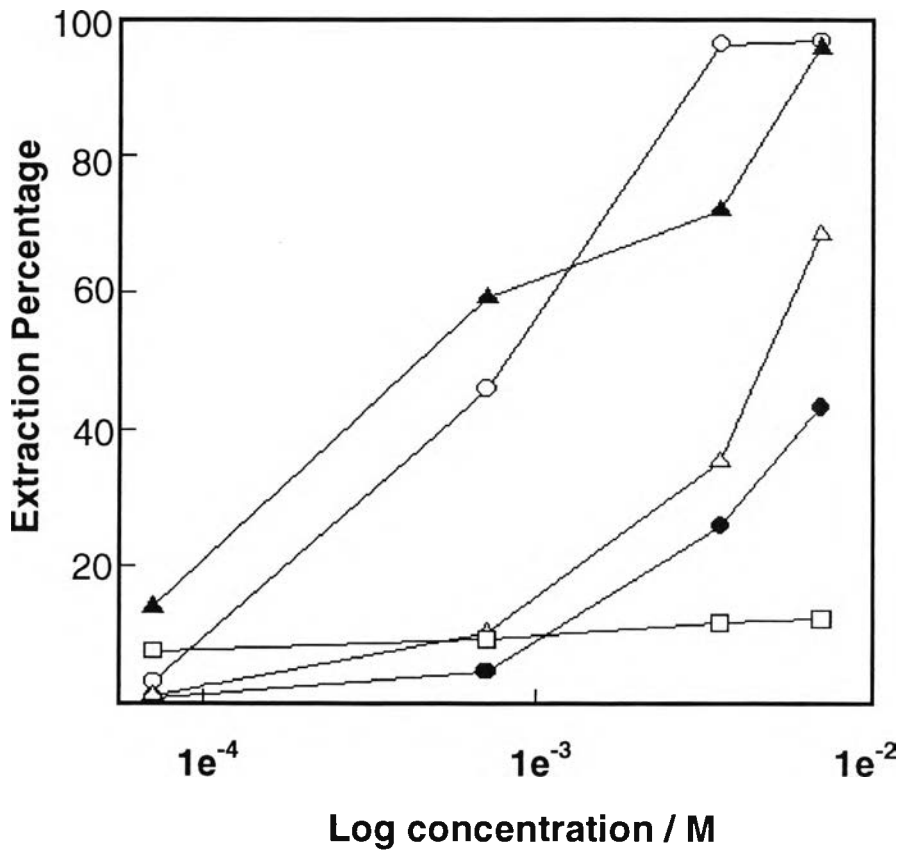

Figure 4.27 Ion extraction of benzoxazine monomers of▲) **1** ; △) **2** ; ○) **3** ; ●) **4** ; and□) **5** ; at monomer concentration of $7x10^{-5}$, $7x10^{-4}$, 3.5 x 10^{-3}, and $7x10^{-3}$ M. sodium picrate salt at concentration $7x10^{-5}$ M.

Figure 4.27 shows that when the concentration of **1**-**5** increases, the sodium picrate extraction percentage is gradually increased. In the case of **1** and **4**, the extraction percentage was nearly 100% while in the case of **5**, the extraction percentage was only 10%.

Chirachanchai *et al.* reported that **1** showed the ion extraction ability with Li^+, Na^+, and K^+ nearly 100% when the concentration of **1** was 0.1 M. In the present work, it was found that **1** gave the ion extraction percentage nearly 100% even using less concentration for 10 times. It should be noted that the ion extraction ability of monomer **1** and **4** started at concentration 10^{-3} while **2**, **3**, and **5** started at $7x10^{-4}$ M. This implied that the molecular assembly of benzoxazine monomer will be formed effectively at above certain concentration. It can be mentioned that the monomer with side groups on benzoxazine unit such as methyl, ethyl, or *t*-butyl gave the higher ion extraction percentage than the monomers without those groups. The result implied that the structure of benzoxazine should play an important role in the ion extraction. Since benzoxazine monomer does not provide the specific cavity by its own monomer unit, the ion entrapment ability may come from the unique molecular assembly.

Considering benzoxazine monomers, the molecular assembly may be formed by stacking conformation between benzene ring, However, the oxygen and nitrogen atoms will make the oxazine ring repulsion owing to the electronegativity. Although, the studies in more details required, especially x-ray single crystallography analysis, it can be mentioned that the bulky group in oxazine gives the loose packing to provide more space than guests.

4.2.2 Effect of Structure of Benzoxazine Monomers

In order to clarify the effect of the structure of monomer on metal ion interaction, a series of monomers were prepared. The ion interaction properties were studied by variation of host-guest ratio.

As shown in Figure 4.28, monomers **5**, **10**, **15**, which are based on phenol, show ion extraction percentage for either K^+ and Na^+, less than 20% even the host concentration was higher than guest concentration for 100 times.

In contrast, Figure 4.29 suggests that **4**, **9**,and **14** having the same basic unit of *t*-butyl phenol, extract high percent of ion only when the amine group was methyl group, **4**. Thus, the results implied effect of aza group containing no bulky group. The extraction percentage was significant.

Figures 4.30 and 4.31 demonstrate that benzoxazines with a series of 2,4 dimethylphenol and 4-ethylphenol have high percent of ion extraction. However, in this case, the ones with methyl group at N (monomer **1** and **3**) showed higher percent extraction than the ones with propyl or cyclohexyl group at N (monomer **6** and **11**). The results informed that benzoxazine increased ion interaction ability when the benzene ring has the bulky group but the nitrogen and oxygen at oxazine ring have less steric effect.

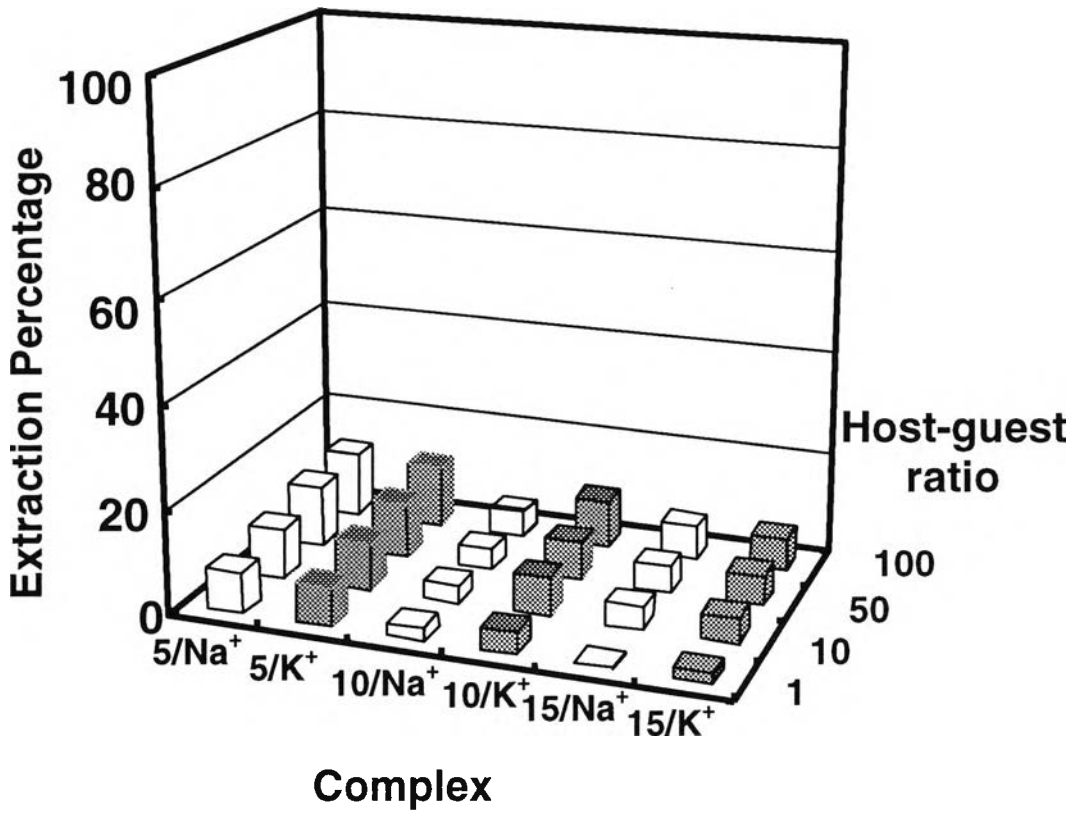

Figure 4.28 Ion extraction percentage of benzoxazine monomers **5**, **10**, and **15** by varying host guest ratio using picrate salt of :Na^+ (white bar) and K^+ (solid bar) at the concentration $7x10^{-5}$M.

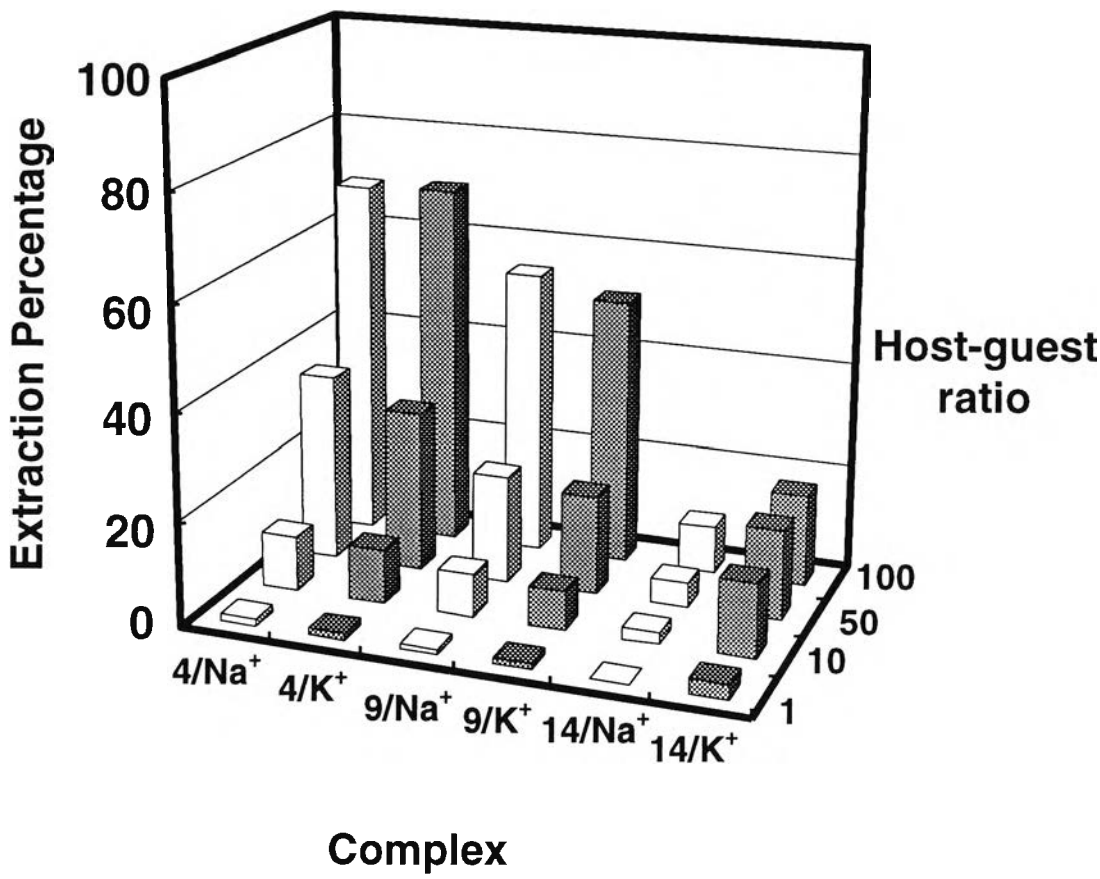

Figure 4.29 Ion extraction percentage of benzoxazine monomers **4**, **9**, and **14** by varying host guest ratio using picrate salt of :Na^+ (white bar) and K^+ (solid bar) at the concentration $7x10^{-5}$M.

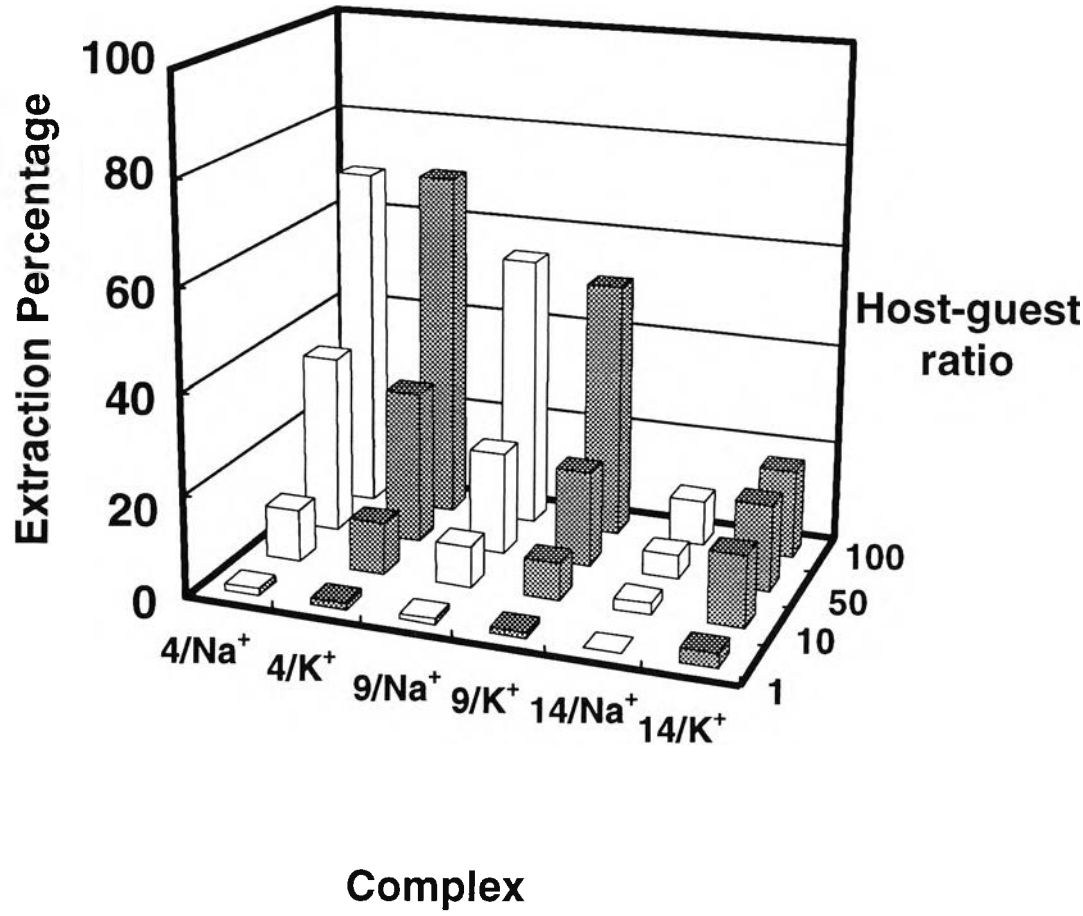

Figure 4.30 Ion extraction percentage of benzoxazine monomers **3**, **8**, and **13** by varying host guest ratio using picrate salt of :Na^+ (white bar) and K^+ (solid bar) at the concentration $7x10^{-5}$M.

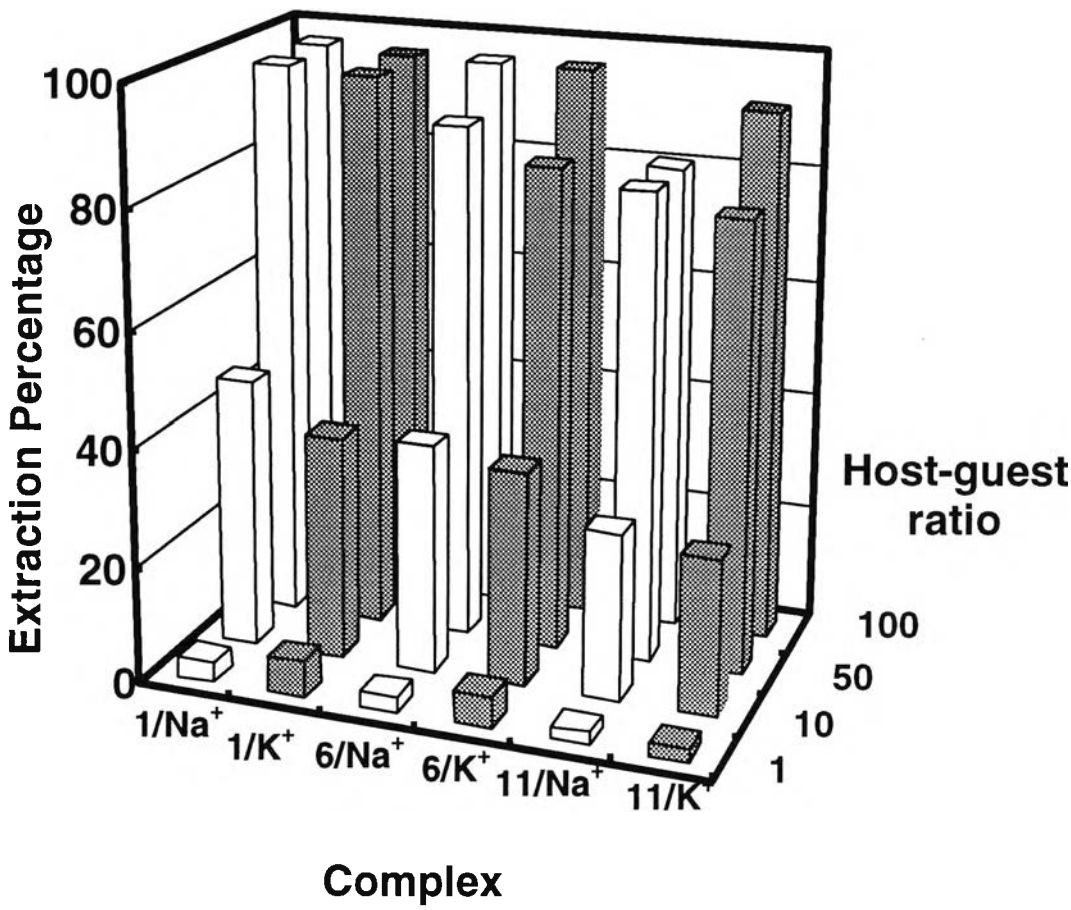

Figure 4.31 Ion extraction percentage of benzoxazine monomers **1**, **6**, and **11** by varying host guest ratio using picrate salt of :Na^+ (white bar) and K^+ (solid bar) at the concentration $7x10^{-5}$M.

4.3 Ion Interaction of Benzoxazine Dimer Derivatives

4.3.1 XRD Analysis

It was noticed that when the $CuCl_2$ aqueous solution was mixed with benzoxazine dimer in organic solution, the color of organic phase was changed to gray-brown, while the blue color of aqueous phase disappeared. This suggested that the host-metal complexation occur in the system. However, for other metal salt solutions, i.e., $BaCl_2$ and $CaCl_2$, which have no color in aqueous phase, after mixing benzoxazine dimers and the salts, both organic and aqueous phases do not show any color.

In order to study the host-guest complexation, the XRD patterns of the prepared samples, i.e., benzoxazine dimer- metal salt- extract and benzoxazine dimer - metal salt - blend, were observed. As shown in Figures 4.32-4.34, the patterns of benzoxazine dimers **16-24** give sharp peaks in the range of 2°-30°, which imply the high crystallinity of benzoxazine dimers.

Figures 4.35 and 4.36 show the XRD patterns of **16**, $CuCl_2$, **16**-$CuCl_2$-extract, and **16**-$BaCl_2$-blend. XRD pattern of **16**-$CuCl_2$-blend (Figure 4.35) shows the combination peaks between **16** and $CuCl_2$, i.e., 13.9°, 20.2°, and 33.6° belonging to $CuCl_2$ and 7.6°, 15.0°, or 19.8° belonging to **16**. We noticed that after grinding salt with **16**, the obtained **16**-$CuCl_2$-blend showed the gray color, though the color of **16** and $CuCl_2$ were white and blue, respectively. The peaks at 6° and 15° of benzoxazine dimer showed the significant decrease in the case of **16**-$CuCl_2$-blend. This might be due to the solid state reaction of **16** and metal salts.

However, for the **16**-$CuCl_2$-extract, a series of totally different characteristic peaks were observed, i.e., 3.9°, 10.6°, and 11.7°. The results suggested that there should be a complexation between **16** and $CuCl_2$, which made the packing structure of **16** changed drastically. In the case of **16** and other metals, i.e., $BaCl_2$, and $CaCl_2$, the XRD patterns turned out to be the

same, which implied the solid state reaction for the cases of benzoxazine dimer-metal salt blend and complexation for the cases of benzoxazine dimer-salt-extract.

Figure 4.37 shows the characteristic peaks of **17** at 6.8° and 10.1°. Here, **17**-$CuCl_2$-extract, **17**-$CaCl_2$-extract and **17**-$BaCl_2$-extract gave absolutely different XRD patterns from that of **17.** It should also be noted that in the case of **17**-$CaCl_2$-extract, the XRD pattern shows pattern similar to **17**-$CuCl_2$-extract and **17**-$BaCl_2$-extract. This implied that when the complexation of benzoxazine dimer with metal ion occurred, the complexation packing structure was change. The packing structure of **17**-$CaCl_2$-extract should be the related structure to **17**-$BaCl_2$-extract and **17**-$CuCl_2$-extract.

Figure 4.41 shows the XRD patterns of **18**-$CuCl_2$-extract, **18**-$CaCl_2$-extract, and **18**-$BaCl_2$-extract. The XRD pattern of **18**-$CaCl_2$-extract was similar to **18**. This meant that the complexation between $CaCl_2$ and **18** occurred while the packing structure was maintained. (This result also can be confirmed by FTIR (see 4.3.2)). It is interesting to find that the **18**-$CuCl_2$-extract and **18**-$BaCl_2$-extract performed the same XRD patterns. This suggested that there be a certain crystal structure of **18**-metal complex.

In the case of **22** - metal salt - extract, XRD patterns show the same (Figure 4.39). This can be mentioned that **22** responded to the metal ion and gave the structure different from the original compound. It was clarified that all types of dimers interact with metal ions, although the complex structure could not be determined in the present work.

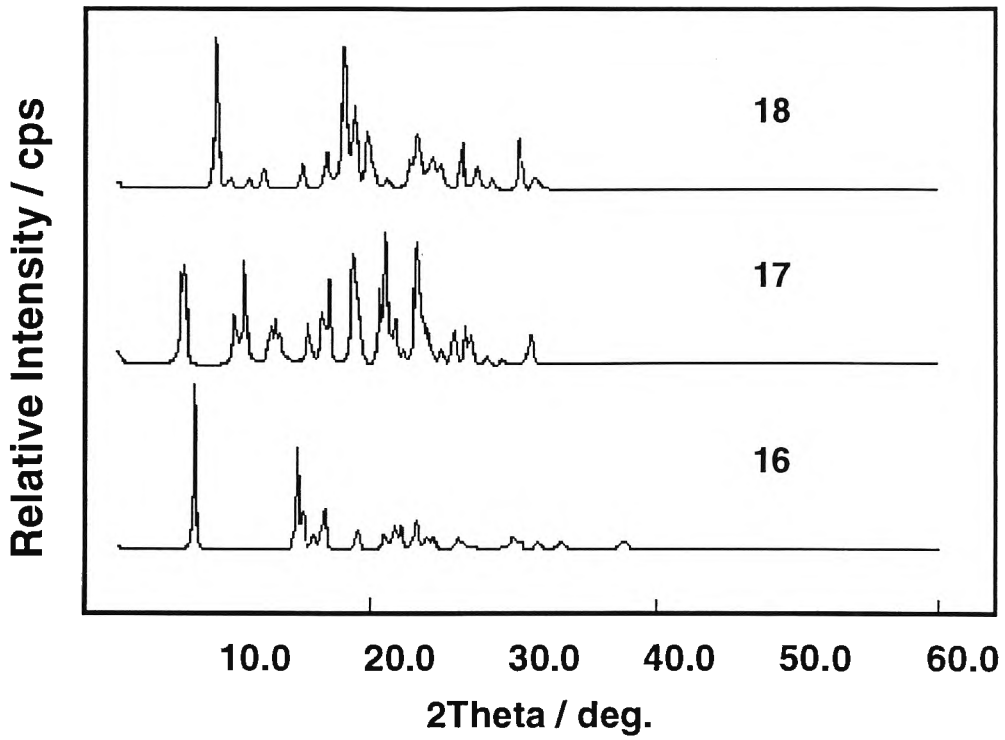

Figure 4.32 XRD patterns of **16**-**18**.

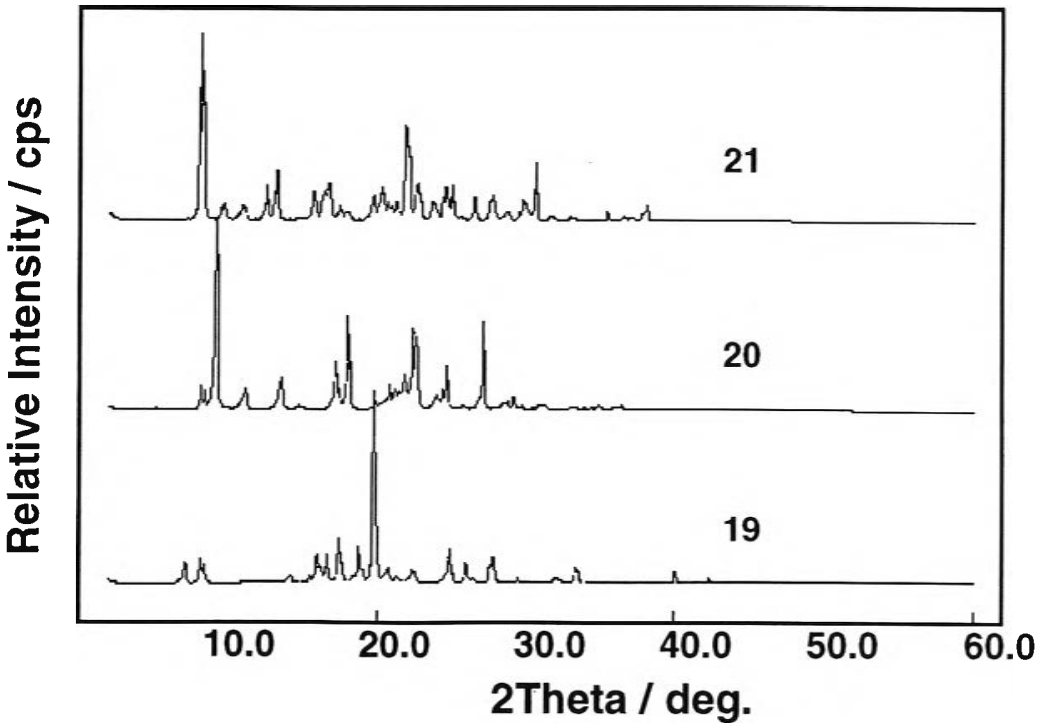

Figure 4.33 XRD patterns of **19**-**21**.

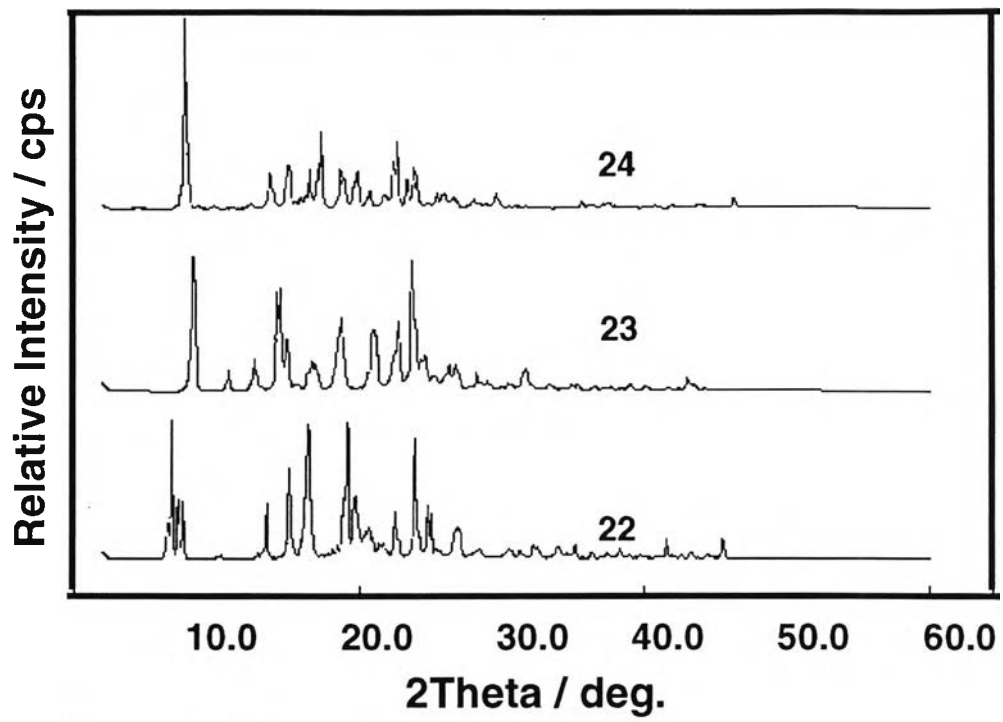

Figure 4.34 XRD patterns of **21**-**24**.

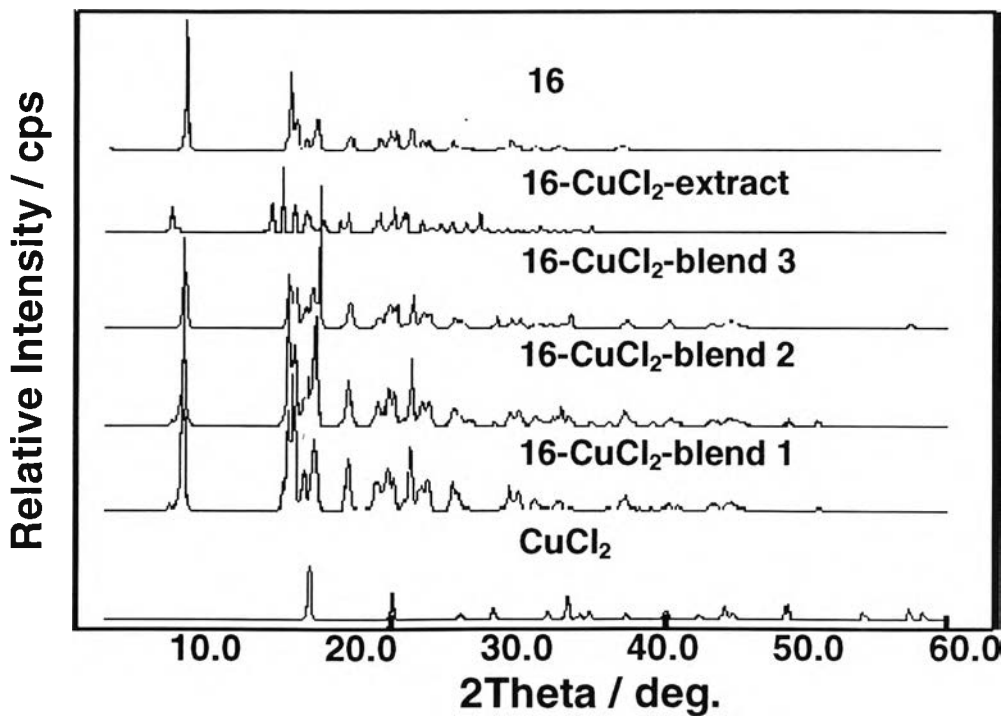

Figure 4.35 XRD patterns of **16**, **16**-$CuCl_2$-extract, **16**-$CuCl_2$-blend 3, **16**-$CuCl_2$-blend 2, **16**-$CuCl_2$-blend 1, and $CuCl_2$.

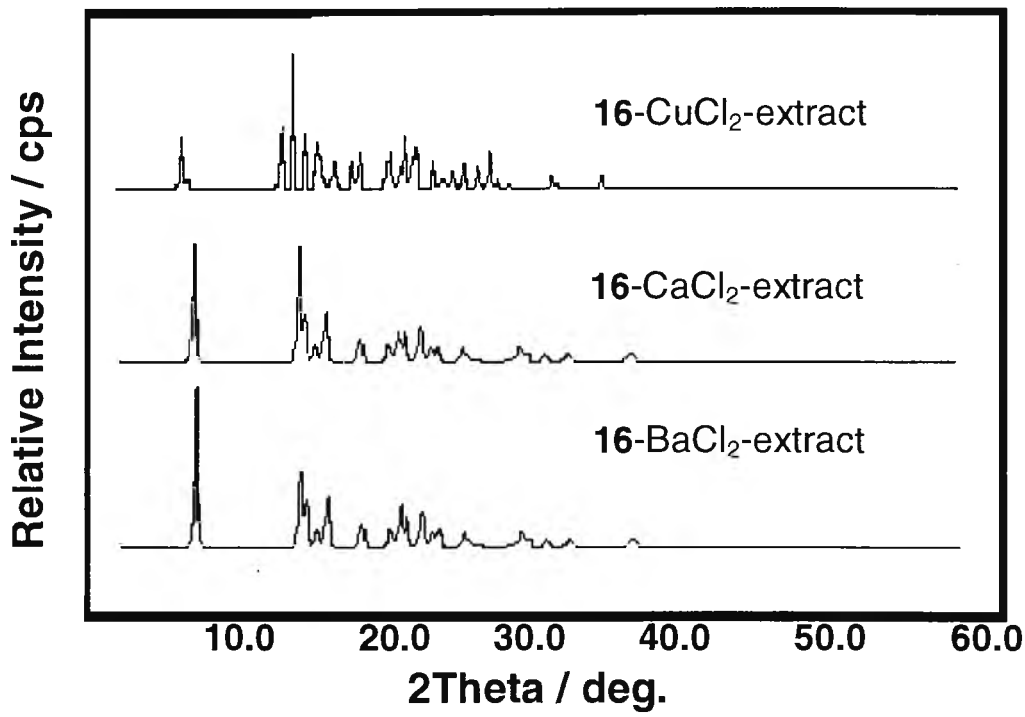

Figure 4.36 XRD patterns of **16**-$BaCl_2$-extract, **16**-$CaCl_2$-extract, **16**-$CuCl_2$-extract.

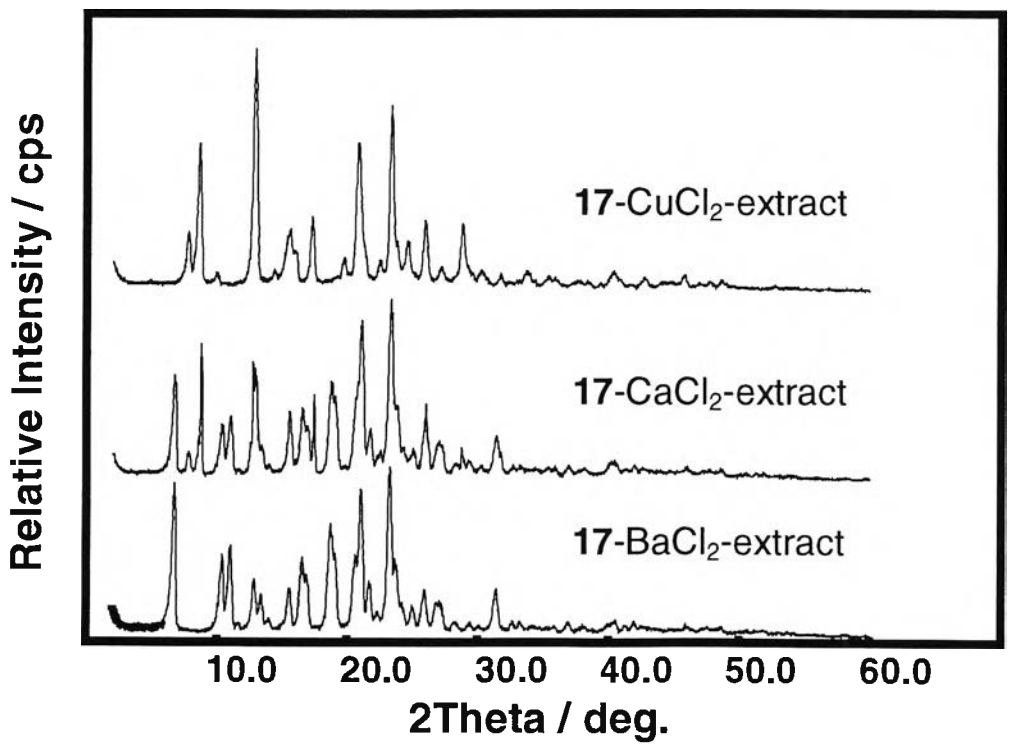

Figure 4.37 XRD patterns of **17**-$BaCl_2$-extract, **17**-$CaCl_2$-extract, **17**-$CuCl_2$-extract.

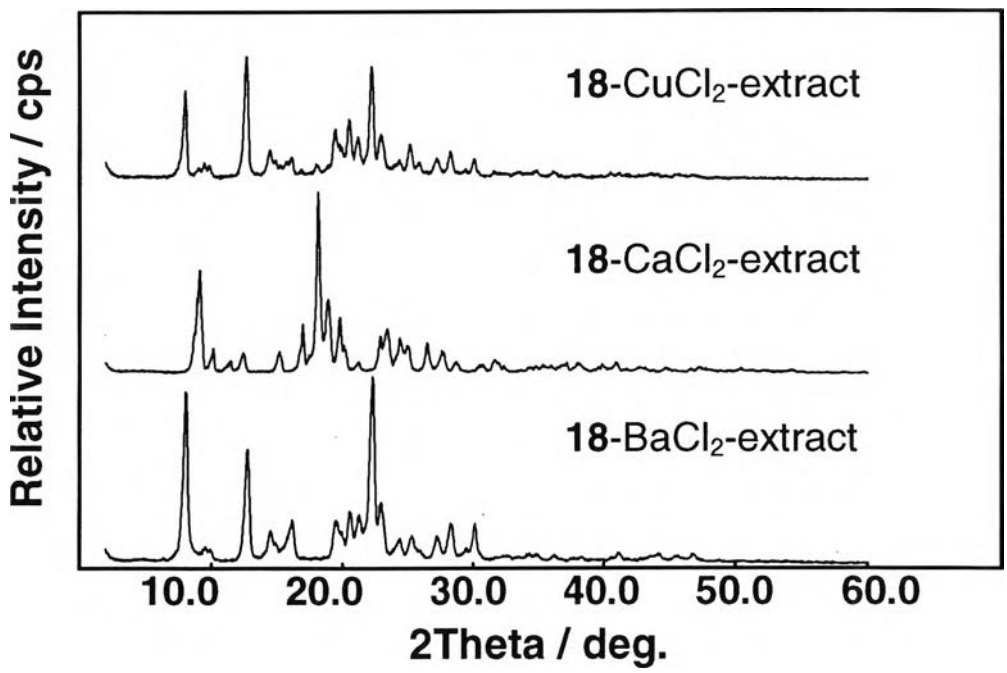

Figure 4.38 XRD patterns of **18**-$BaCl_2$-extract, **18**-$CaCl_2$-extract, **18**-$CuCl_2$-extract..

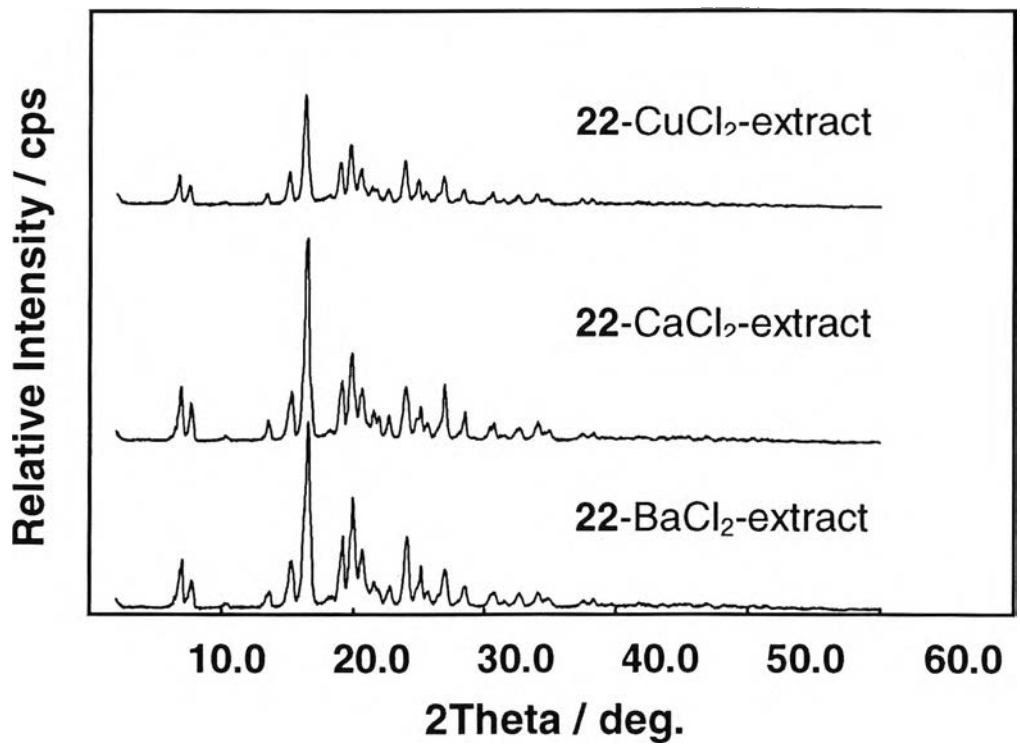

Figure 4.39 XRD patterns of **22**-$BaCl_2$-extract, **22**-$CaCl_2$-extract, **22**-$CuCl_2$-extract.

4.3.2 FTIR Analysis

FTIR was applied to study the structure of benzoxazine dimers and complexes. Since the complexation of organic compound and metal ion is known to be formed and controlled by the amount and the position of lone pair electrons, the functional group related to the nitrogen and oxygen should show the peak shift from the original compound. Figure 4.40 shows that the spectra of **17**-$CuCl_2$-extract, **17**-$CaCl_2$-extract, and **17**-$BaCl_2$-extract and **17** are different. Considering **17**-$CuCl_2$-extract, **17**-$CaCl_2$-extract, and **17**-$BaCl_2$-extract, each of the extract shows O-H stretching at 3366, 3318, and 3290 cm^{-1} respectively, while **17** shows at 3304 cm^{-1}. This implied that hydroxyl group, especially oxygen atom of **17**, played an important role in complexation with metal ions. Techakamolsuk *et al.* reported that benzoxazine dimers formed intramolecular hydrogen bonding between the hydroxyl OH and aza group. Here, it should be noted that when **17** formed the complex with metal ion, the intramolecular hydrogen bonding was changed, especially in the case of $CaCl_2$, as observed from the peaks around 3050-3150 cm^{-1}.

In the previous part, we discussed about the complexes of **18**. FTIR shows the significant change in the OH peak, i.e., from the intramolecular hydrogen bonding peak to free hydroxyl peak (Figture 4.41). The complex with $CaCl_2$ gives sharper peak of hydroxyl group than others. It is interesting to note that **18**-$CuCl_2$ gave the peak splitting which implied that the C=C conjugation also played the role in complexation.

Chirachanchai *et al.* (in preparation) reported that all of the benzoxazine dimers have intramolecular hydrogen bonding as observed from the single crystal analysis. The complexation should be induced controlled by the lone pair electrons of OH and N, while the former intramolecular hydrogen bonding was eliminated. The dimer conformation was another important point to be discussed. In the case of **16**, the planar of two benzene

rings are widely open, while two benzene rings of **17** show the stress and the bending of each ring to each other as referred to Chirachanchai *et al.* (in preparation). This may be the reason why the complexation of **17** is more significant than other types. The FTIR of **17** comparing to its complex is another evidence to support this explaination.

Figure 4.42 shows **22** and the 22-metal-extract, which the hydroxyl peaks are shifted and C-N peaks are also changed. This implied that **22** formed the complex with Ba^{2+}, Ca^{2+}, and Cu^{2+}.

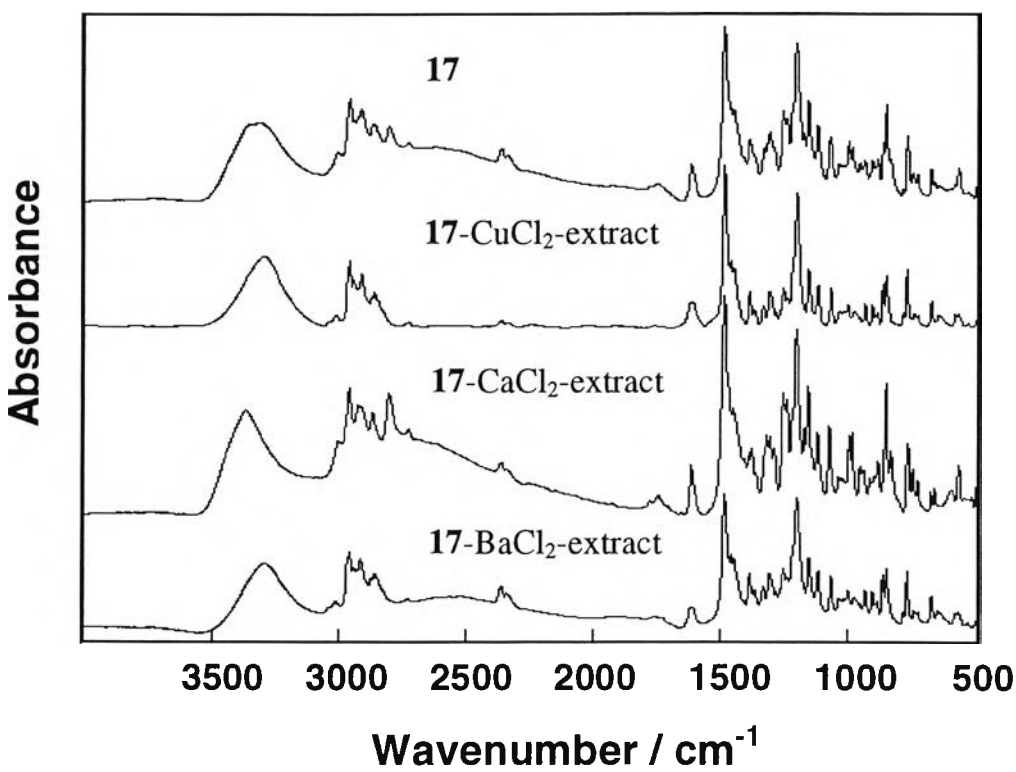

Figure 4.40 FTIR spectra of **17**, **17**-$BaCl_2$-extract, **17**-$CaCl_2$-extract, and **17**-$CuCl_2$-extract.

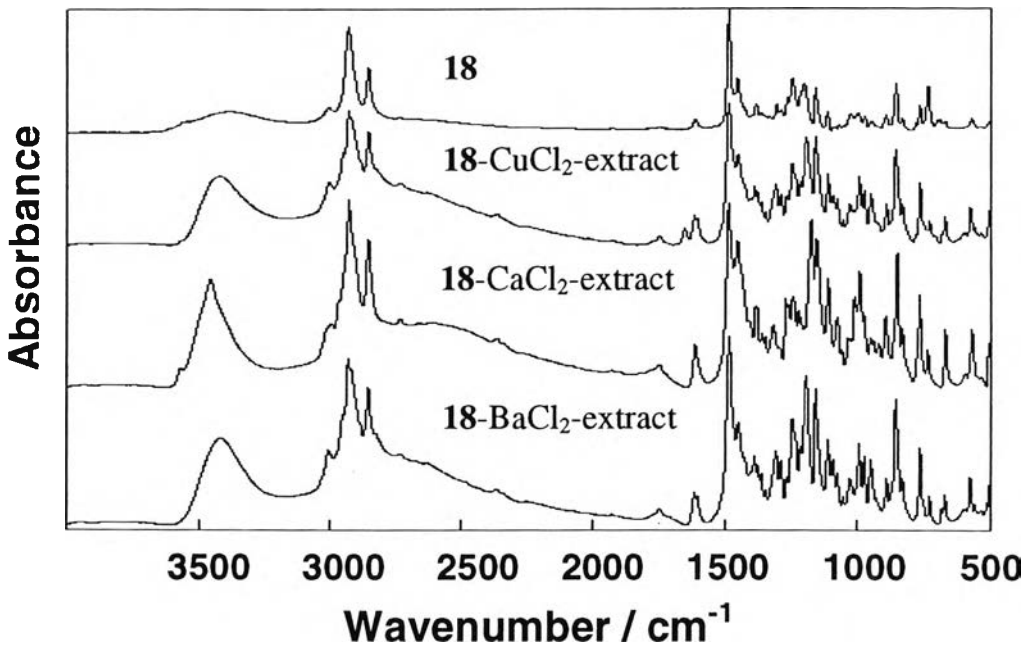

Figure 4.41 FTIR spectra of **18**, **18**-$BaCl_2$-extract, **18**-$CaCl_2$-extract, and **18**-$CuCl_2$-extract.

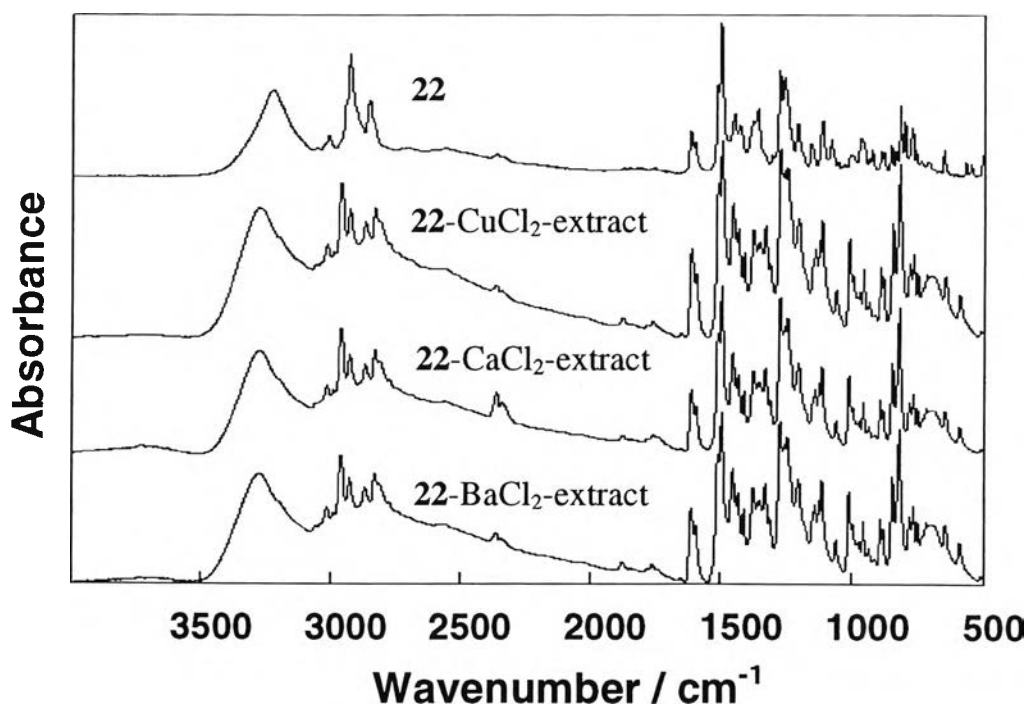

Figure 4.42 FTIR spectra of **22**, **22**-$BaCl_2$-extract, **22**-$CaCl_2$-extract, and **22**- $CuCl_2$-extract.

4.3.3 ESIMS Studies

According to the concept of host guest compound, it is necessary to clarify that benzoxazine dimers present as an assembly including the metal ion as a guest. Since ESIMS is a technique for quantitative analysis of protein, protein-metal complex, and the noncovalent bonded ligand, it is our interest to apply this technique for identification the of assembly.

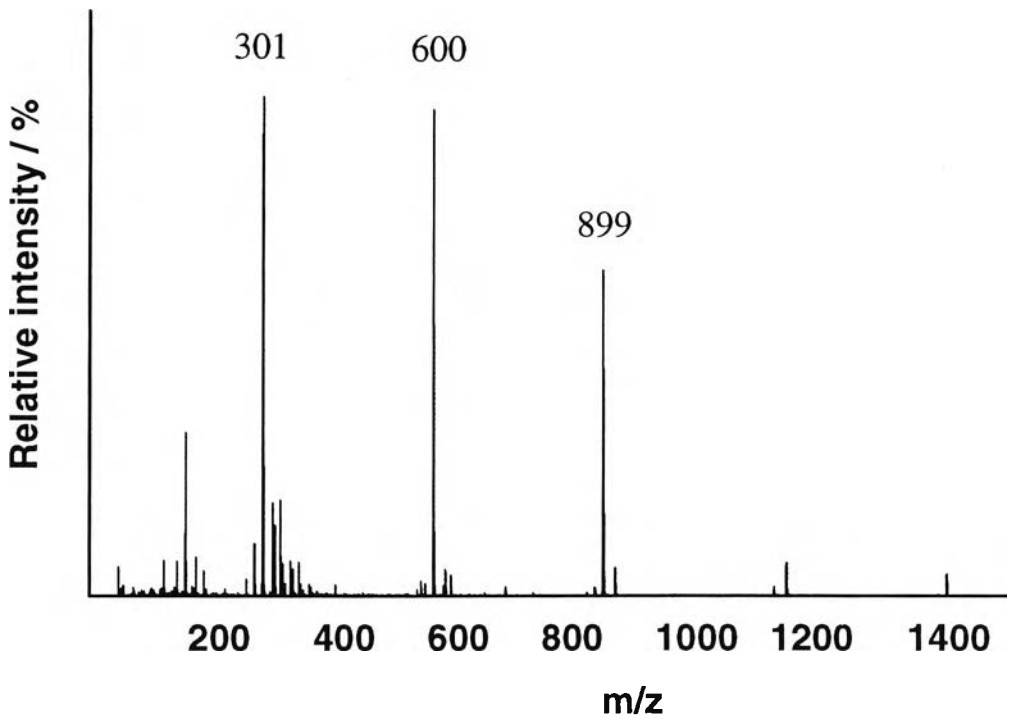

Figure 4.43 ESIMS spectrum of **22** when the orifice was 35 V.

Figure 4.43 shows mass spectrum of pure monomer **22** at orifice voltage 35 V in methylene chloride solution. The peak (M+H) at m/z = 300, which is equal to the molecular weight of dimer **22**, was observed. Meanwhile, there are a series of peaks appearing at the m/z = 600, 899, and 1200. Considering the intensity, the two and three molecules of **22** were presented as main species in the solution. It is known that ESIMS is a technique to determine MW of low MW species (<2400) in solution state under the low ionization potential energy. In this case, not only the molecule

of the complex but also the aggregation or the cluster can be observed. Thus, the peaks at 600, 899,1200 suggested the assembly of two, three, four and five molecules of the dimer **22**. However, when the applied voltage was 70 V, the relative intensity of high m/z peaks, such as m/z = 600, 899 and 1200, were decreased. This due to the high ionization potential broke the self-assembly of **22**. The observation of m/z at 164 indicated that one side of benzene ring of dimer was removed out as proposed in Scheme 4.1 (a). This might be because the intramolecular hydrogen bonding stabilized this fragment. The peak at 135 suggests the dissociated fragment shown in Scheme 4.1 (b).

Scheme 4.1 Fragment species of 22 under orifice voltage 35 V.

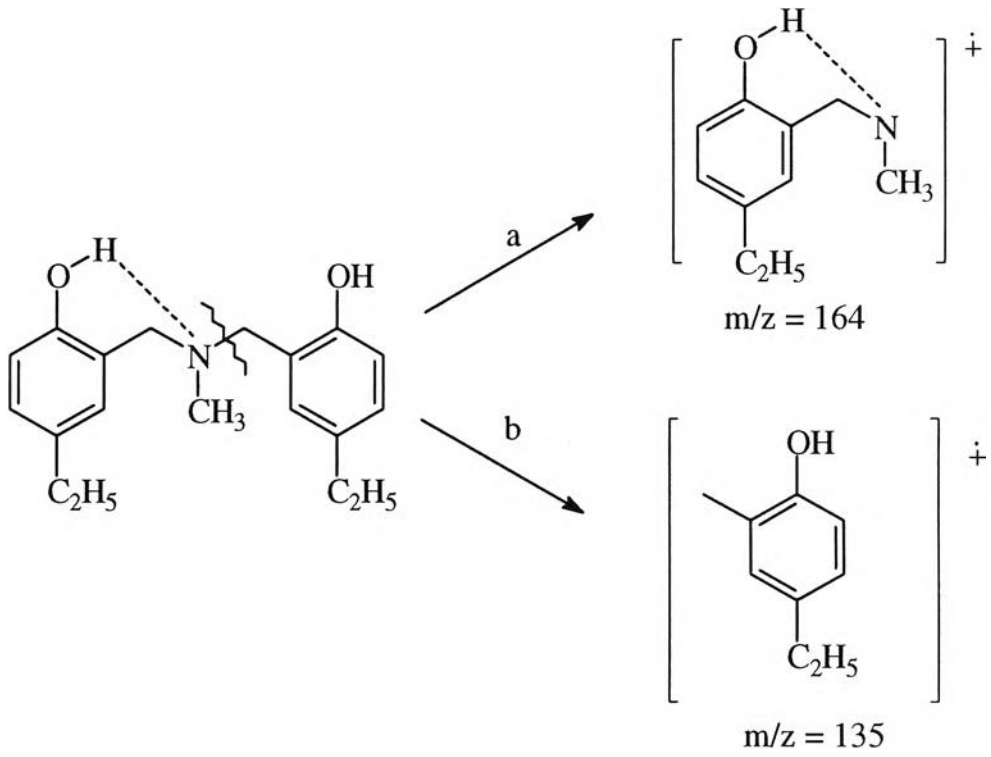

The peak m/z at 166 indicated that one benzene ring was removed as proposed in Scheme 4.1 (a). This proposed scheme is also supported by the evidence of intramolecular hydrogen bonding formed in the structure.

Another fragment observed at m/z 135, suggested the dissociated species shown in Scheme 4.1 (b).

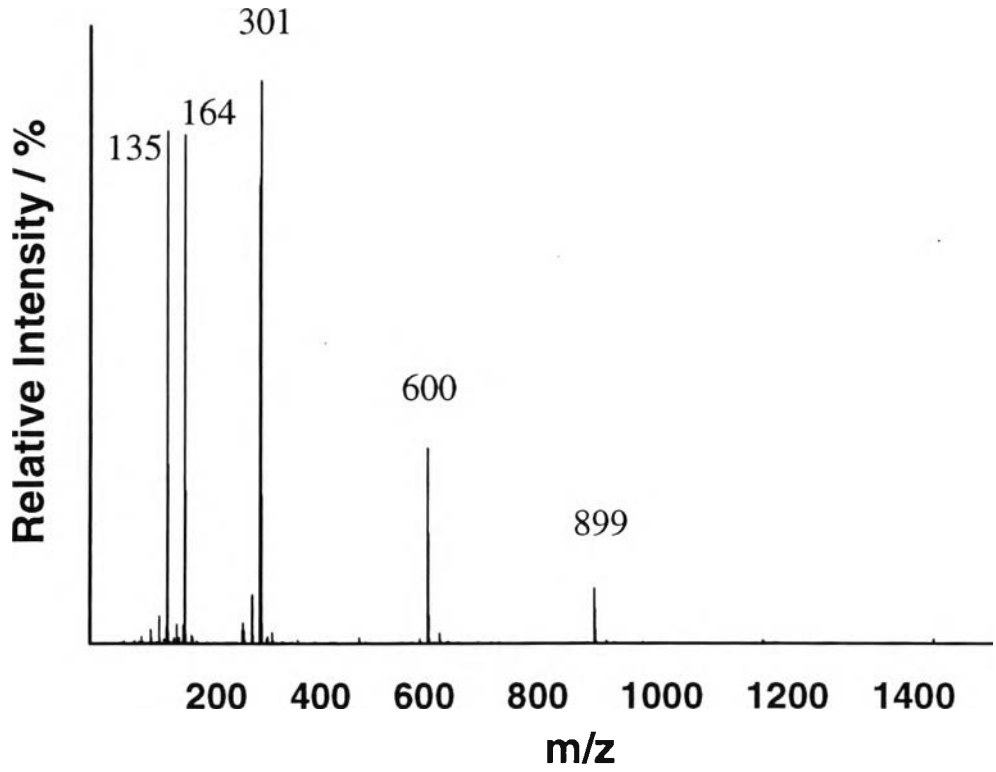

Figure 4.44 ESIMS spectrum of **22** when the orifice was 70 V.

In the high voltage, at 110 V, the more fragments were generated than in the case of the applied voltage at 35 and 70V. This implied the same fragmentation, as shown in Figure 4.45.

According to the results, the applied voltage at 35 V was found to be appropriate to study the self-assembly of **22**. Thus, the benzoxazine dimer and metal host guest complexation was operated under the applied orifice voltage 35 V.

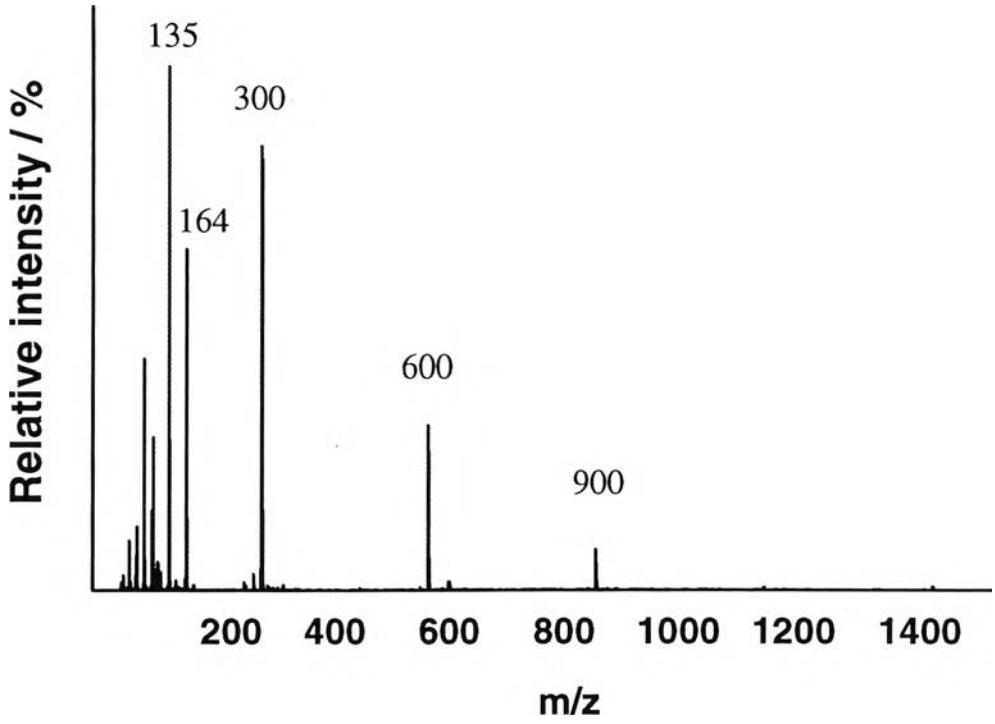

Figure 4.45 ESIMS spectrum of **22** when the orifice was 110V.

The complexation of **22** and metal ions are shown in Figure 4.46. It is pointed that **22**-$BaCl_2$-extract at applied voltage 35 V did not show the same dissociated fragment as found in Figure 4.43. The fragmentation of **22**-$BaCl_2$-extract indicated that the compound formed the cluster as twice to seven times of dimer molecules. The characteristic peaks are meant for the complexation between **22** and barium ion were found at m/z = 737, 1492 and 2230.5. Since the atomic weight of Ba is 139.5 and the molecular weight of dimer **22** is 299, the peak at m/z = 737.5 suggested the combination of two dimers and one metal ion. Moreover, m/z = 2230.5 was also enhanced and can be referred to the complexation of **22** and metal ions. The maximum aggregation observed from the ESIMS was at m/z = 2230.5. This peak represented the mass of seven dimers with one metal ion. However, the peak at m/z = 1492 implied the aggregation of five benzoxazine dimers which did not include the guest.

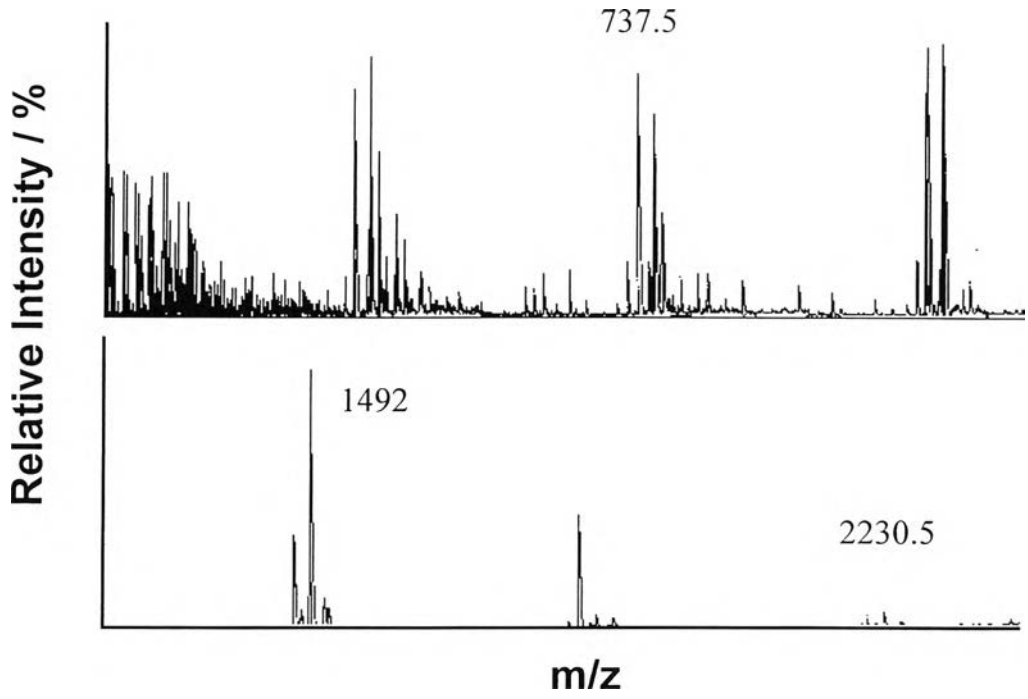

Figure 4.46 MS spectrum of **22** + $BaCl_2$. when the orifice was 35V.

Figure 4.47 confirmed the complexes of cupric ion and **22** showing the characteristic peaks at m/z = 900, 961.5, and 2097. The observed peaks were related to the cluster three dimers and seven dimers as self-assembly structures. Comparing the spectra between pure dimer **22** and metal-host, it was found the peak positions of **22** combined with metal at 961.5. The peak 961.5, thus, was referred to the combination of three dimers and one metal ion.

In order to compare the effect of ionization potential energy to the metal complexation, **22**-$CaCl_2$-extract was studied under the orifice voltage values, 35 V and 70 V At the lower one (Figure 4.48), the maximum peak of m/z 2097 was referred to seven dimers aggregation. The spectrum showed the cluster formation of the monomers in the range of two to seven dimer at m/z = 300, 599, 899, 1198, 1498, 1898, and 2097 cm^{-1}, respectively.

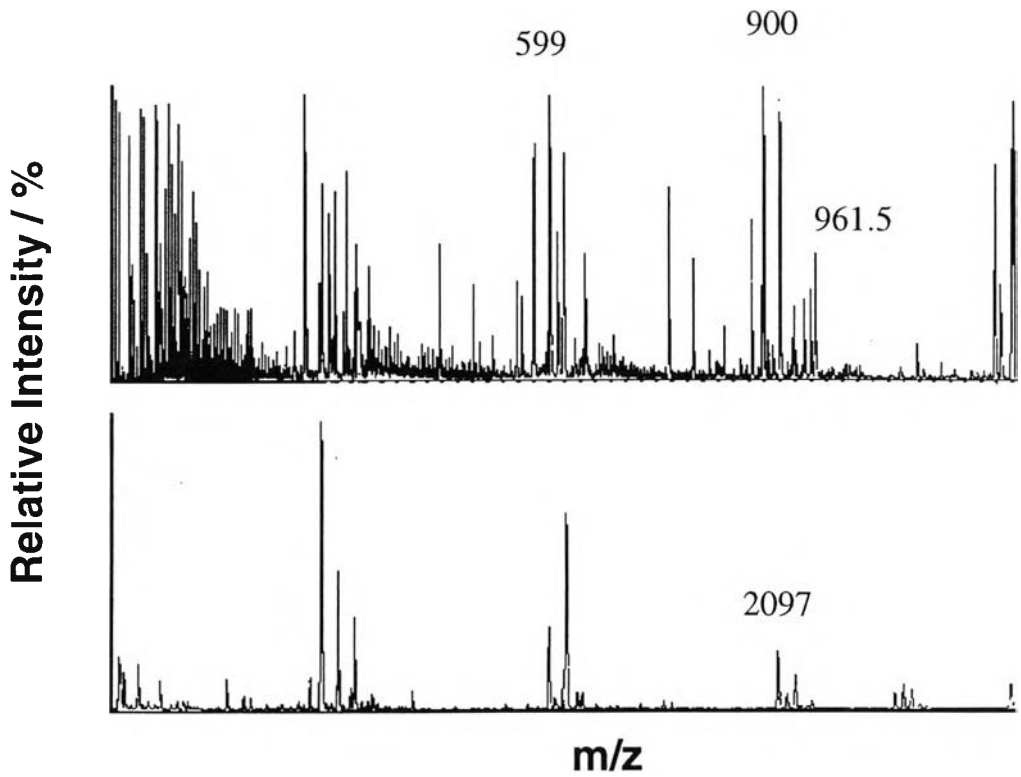

Figure 4.47 MS spectrum of **22** + $CuCl_2$ when the orifice voltage was 35 V.

Figure 4.49 displays the decreasing of the m/z number at high value. The peaks at above m/z = 1500 disappeared while peaks at 1497 and 899 were decreased for the intensity, significantly.

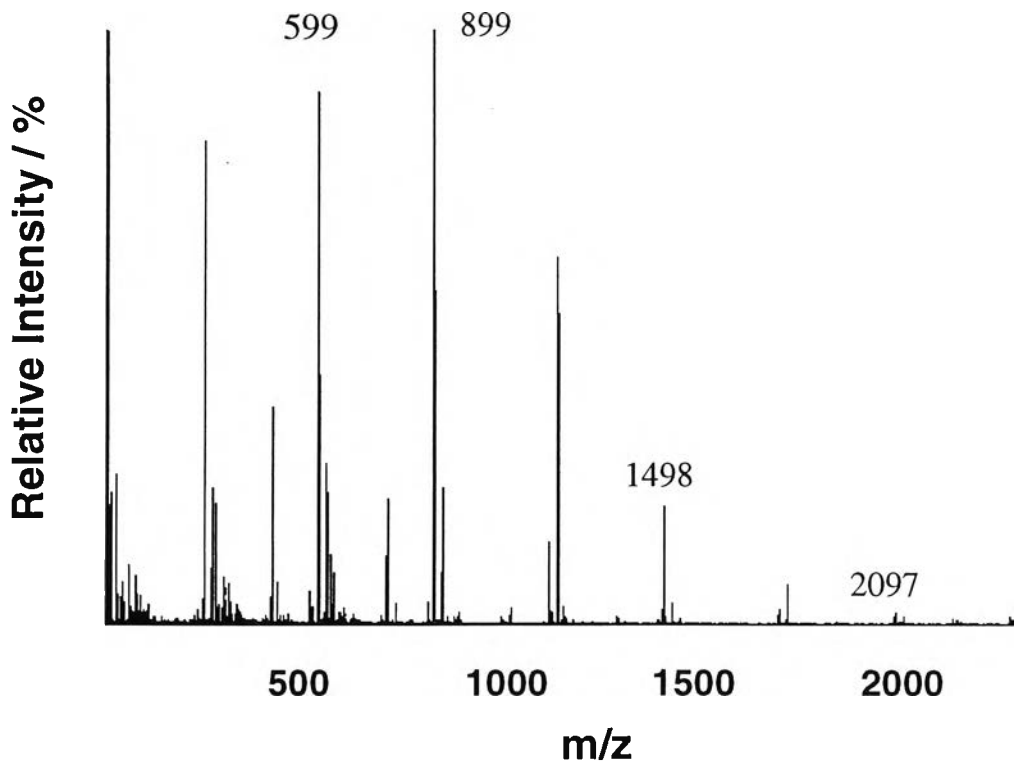

Figure 4.48 MS spectrum of **22** + $CaCl_2$ when the orifice voltage was 35 V.

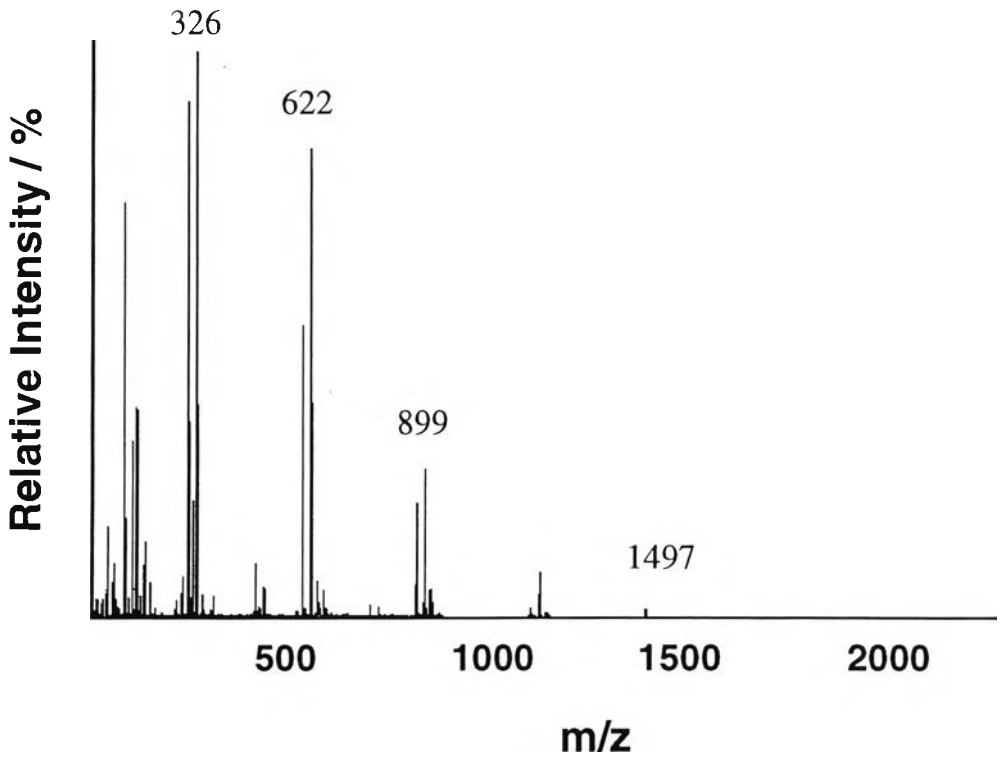

Figure 4.49 MS spectrum of **22** + $CaCl_2$ when the orifice voltage was 110V.